THE DESIGN AND DEVELOPMENT OF OSTEOINDUCTIVE AND OSTEOCONDUCTIVE PRE-VASCULARISED 3D PRINTED SCAFFOLDS WITH HIGH POROSITY AND LOAD BEARING PROPERTIES FOR BONE REGENERATION

By

ADHITHI KANTHAN LAKSHMIKANTHAN

A thesis submitted to the

School of Graduate Studies

Rutgers, The State University of New Jersey

In partial fulfillment of the requirements

For the degree of

Master of Science

Graduate Program in Biomedical Engineering

Written under the direction of

Joseph Freeman

And approved by

_____

_____

_____

_____

New Brunswick, New Jersey

January – 2018

ABSTRACT OF THE THESIS

THE DESIGN AND DEVELOPMENT OF OSTEOINDUCTIVE AND OSTEOCONDUCTIVE PRE-VASCULARISED 3D PRINTED SCAFFOLDS WITH HIGH POROSITY AND LOAD BEARING PROPERTIES FOR BONE REGENERATION

By ADHITHI KANTHAN LAKSHMIKANTHAN

Thesis Advisor:

Joseph Freeman

Due to increased life expectancy and needs of the baby boomer population, it is estimated that in the United States alone, 1 million patients annually would require bone defect repair by 2020. The solution for bone regeneration is bone grafting. Autografts, allografts and xenografts have their disadvantages out weighing the benefits. Synthetic grafts are the latest alternative to overcome most of these issues such as donor site morbidity, bone shortage, high costs, transmission of infections, and ethical concerns. However, most current bone graft options fall short of managing the tight rope between mechanical properties, scalability, vascularization and porosity. Our lab has previously fabricated implants that have cortical sections modeled based on the structure of osteons. This project focuses on building on that initial design and 3D printing highly porous, pre-vascularized, osteoconductive and osteoinductive, load bearing scaffold for bone regeneration. Presence of micro-pores and macro-pores are seen. Trabecular sections have pores measuring 300-350 μm which is known to support bone growth, and the whole scaffold has pores approximately 5 μm in size which is favorable for vascularization. The scaffolds have good mechanical strength and are further reinforced using structural posts made of hydroxyapatite. Using 3D printing technology ensures greater control over the structure, porosity and pore size,

and also reduces time, effort and human error. Thus the results of this project display the ability of a porous scaffold to develop new bone and vasculature while bearing physiological load that is cost effective, scalable, easily reproducible and a clinical reality.

DEDICATION

To ma and pa, who am I but your daughter?

TABLE OF CONTENTS

LIST OF FIGURES

LIST OF TABLES

CHAPTER 1 – Introduction

1.1 Bone structure, function and composition

Bone is a dynamic 3D structure made of the ultimate smart material, with rapid mineralization properties. It is capable of self-healing and remodeling without leaving a scar and is highly vascularized. [62] It provides structural support to the body, is load bearing, acts as mineral reservoir, supports and protects the internal organs. [62] Apart from these basic functions, bones are also involved with housing biological components required for hematopoiesis, and trapping dangerous metals such as iron. [68]

Structurally, bone is categorized into a porous trabecular region and a highly compact cortical region. [19] The human skeleton comprises of only 20% trabecular bone, and 80 % of cortical bone. 90% of the trabecular bone, however, comprises of pores, while only 20% of the cortical bone is made of pores. This is why cortical bone has mechanical strength and stiffness compared to that of trabecular bone. [62] Toughness (strength) of bone is due to the organic matrix composed of type I collagen, whereas the stiffness (modulus) and viscoelastic behavior of bone is due to the hydrated inorganic mineral phase composed of hydroxyapatite (HAp) and water. [19] This is also why bone is a composite - due to the presence of the bone matrix that has the two parts, the inorganic hydroxyapatite part (60-75%) and the organic part (25-30%) [62]

1.2 Bone injury and healing

Bone formation and resorption are coupled processes. Bone remodeling is a process of continuous resorption and neo-synthesis of bone that determines bone structure and quality. [34]
Bone regeneration involves bone induction and conduction, interaction of different cell types, intracellular and extracellular signaling pathways in a temporal and spatial sequence to optimize and repair skeletal function without scar formation. [59, 60] An instance of bone regeneration is

fracture healing. Injured and damaged bone has the ability to heal naturally *unless* there is a significant bone loss. [19] When this fracture doesn't heal correctly, bone regeneration fails, surgical intervention and bone grafts are required.

Broken bones/fractures are one of the most common orthopedic problems, 6.8 million cases are reported annually in USA. [13] Approximately 13% of tibial fractures are associated with delayed or fracture non-unions. [61] Non-union or critical sized defect is a serious complication wherein bone healing process is interrupted due to the fracture moving too much, has poor bloody supply or gets infected. [71] 1 million cases of skeletal defects a year require bone grafts to achieve union. [4]

Due to increased life expectancy and needs of the baby boomer population, it is estimated that in the United States alone, 1 million patients annually would require bone defect repair by 2020. [69] A wide range of orthopedic applications and skeletal reconstruction requires bone grafting. Some of these defects are calvarial defects, anterior spine fusion, acetabular defects, cystic lesion femur condyle metaphysis, ankle joint arthrodesis, osteolytic/traumatic long bone defects, ilial defects, maxillary defects, zygomatic bone defects, trauma, infection, tumor resection, birth abnormalities, osteoporosis, compromised regeneration and avascular necrosis. [36], [37-42], [61], [78].

Factors such as location of defect, and patient habits such as smoking also determines bone healing effectiveness after treatment. Smoking has been shown to cause revision requirement due to non-unions. [5]

1.3 Bone Tissue Engineering

Langer and Vacanti define Tissue Engineering as an interdisciplinary field of research that applies the principles of engineering and the life sciences towards the development of biological substitutes that restore, maintain or improve tissue function. [30]

Bone Tissue Engineering or BTE is a complex and dynamic process that initiates with migration and recruitment of osteoprogenitor cells followed by their proliferation, differentiation, matrix formation along with remodeling of the bone [62, 68]. The field of bone tissue engineering gained prominence in 1980's due to its advantages in regenerative medicine, and is gaining importance with every new invention. [30] It comes as no surprise that the orthopedic devices market will see steady growth to cross 53 billion USD by 2024. [15] BTE is looked upon to provide alternate solutions to problems such as stress shielding, low mechanical properties, vascular insult of implant, improving synostosis between implant and tissue at the microscale, osteopenia and subsequent re-fracture. This is especially useful in areas such as reconstructive orthopedics. [29]

The Bone Tissue Engineering paradigm highlights the most important aspects for bone regeneration. The four pillars of the paradigm are a biocompatible scaffold, osteogenic cells to lay down bone tissue matrix, morphogenic signals that help direct the cells to the desirable phenotype, and finally, vascularization to meet oxygen and nutrient needs. These pillars are required to accelerate cell homing, vascularization and bone formation at the defect site. [68]
Of late, the fastest growing segments in the U.S. orthopedic biomaterials market are the stem cell bone graft and concentrated bone marrow markets. Though DBM and synthetics have improved in effectiveness, stem cell grafts are seeing the greatest growth within the orthopedic biomaterial bone graft market. This is in large part due to the fact that stem cells offer the greatest regenerative potential for healing bone. [12] This project utilizes stem cells to satisfy one of the BTE paradigms.

1.3.1 Bone scaffold

Scaffolds are 3D porous solid biomaterials designed to degrade at a controlled rate, promote cell-biomaterial interactions, cell adhesion, ECM deposition, and, transport of gases, nutrients and regulatory factors. Scaffold degradation rate must match tissue growth rate in vitro as well as in vivo. [49]

Bone scaffolds are also the basis for osteoconduction without which no progress can be made. Scaffolds must be also be biocompatible, which implies that the material shouldn't demonstrate immunogenicity or cytotoxicity, neither should it elicit an unresolved inflammatory response. The scaffold's biocompatibility is determined by its chemistry, structure, morphology, polymer synthesis, scaffold processing, and sterilization conditions. [57] Surface properties of scaffolds such as surface to volume ratio are very important for optimal cell adhesion. [51] An ideal bone substitute has high osteoinductive and angiogenic potentials, biological safety, low patient morbidity, no size restrictions, ready to access surgeons, long shelf life and reasonable cost. [68] The world scaffold element technology market was approximately 457 million dollars in 2013, and by growing 13.4% annually, the market will expand to 1.063 billion dollars in 2020, which shows the rising importance of this aspect of tissue engineering. [14]

Osteoinductivity is the ability of a material to promote osteoprogenitor cells into osteoblasts. However, it isn't exclusively dependent on the biomaterial; it weighs equally on porosity and the surficial properties like topography. [62] It also pays to remember that cells are inherently sensitive to their surrounding topography at the micron and nanoscale such as grooves, wells, ridges and other features. Thus, scaffolds should have appropriate porous and surface cues. It is important to design scaffolds that are 'non-uniform'. Uniform scaffolds do not support cell adhesion in the center and therefore less bone is formed, which leads to implant failure due to weak mechanical properties. [29], [31]

PLA is a degradable polymer that is known to exhibit bulk degradation properties and therefore it is also imperative to study and maximize scaffold's mechanical properties and sterilization to prevent infection. [56] The scaffold must have mechanical capabilities to bear the post implantation load and stress, which new tissue being formed will ultimately bear. Further, the scaffold must support a controlled interconnected porous network for optimal cell growth and vascularization. This interconnected geometry ensures a large surface area for cell ingrowth, uniform cell

distribution, and formation of new blood vessels through the scaffold. [52] It also ensures that cells are within 200 μm from blood supply for mass transfer of oxygen, nutrients, and waste products. [56] Finally, a near-net shape scaffold design is preferred, with scalability in a manufacturing scenario.

Thus the golden solution for BTE is to fabricate scaffolds that match the mechanical properties and anisotropy of bone, [32] and recapitulate the complex temporal sequence and combination of GFs involved in safe and stable bone formation in vivo. [32]

It has been seen that complications arising from bone grafting treatments are highly correlated with the site of the bone defect rather than the graft material. [5] Therefore it is crucial to develop and test scaffolds for multiple locations. This is easily possible with rapid prototyping technology such as FDM which is used in this project. The design can be scaled up or scaled down as per requirement.

1.3.2 Bone porosity and vasculature

Vascularization has a strong correlation to the success of a bone graft – it is hypothesized as the initiating factor in new bone formation, and is known to contribute towards bone development, growth and repair. [64] One of the crucial steps in bone healing is angiogenesis or the formation of blood vessels from existing ones. On the other hand, an excess of angiogenesis is harmful too. It might lead to tumor progression. [76]

In this project pre-vascularization is done by seeding scaffolds with HMECs as it has been demonstrated by groups that endothelial cells can generate organized and well connected endothelial vessels throughout 3 dimensional tissue constructs. [34]

Angiogenesis is affected by scaffold porosity and pore size, growth factor transportation, cell response to growth factors and most importantly growth factor control. Blood vessel infiltration into scaffold is of utmost importance, if it is only a few μm in, it's of no use as it leads to lesser or

lack of bone cells deeper inside the scaffold and healing doesn't occur. This in turn implies that the rate of scaffold degradation would not match the rate of bone growth. [76]

Literature suggests different optimal pore sizes for different cells, 200-350 µm for osteoconduction, and 5 µm for neovascularization. [54, 55] Other pore related considerations include pore shape, distribution, orientation, wall roughness, interconnectivity, volume etcetera. [53] As mentioned for osteoconduction, the minimum pore size is 100 µm, and ideal is 200-350 µm. However, it might be better to have both micro (less than 20 µm) as well as macro pores (more than 100 µm). [77]

1.3.3 Mechanical behavior of bone

One of bone's basic functions is that of load bearing, and it is of critical importance to design scaffolds with similar compression values. This ensures proper and optimal bone growth, quality of care for patients, and avoiding re-fracture.

Bone's ability to handle stress i.e. mechanical properties or strength depends on age and gender. Fracture toughness or ability to resist micro crack resistance as well as propagation, increases till 35 years of age in males and 30 years of age in females and then starts decreasing. Bone mass loss also compromises mechanical stability. Repetitive loading conditions cause fatigue damage which results in fragile fractures; this could be due to traumatic load or non-traumatic load (osteoporosis).

Fracture due to compression in cortical bone is dependent on mechanical properties, structure and, bone tissue volume fraction. Young's Modulus of cortical bone is 15-20 GPa and it's compressive strength is in the range of 100-200 MPa. Young's Modulus of cancellous bone is 0.1-2 GPa and it's compressive strength is 2-20 MPa.

One of the most important requirements of BTE is to have grafts with good mechanical properties such as compressive yield strength or strength, ultimate compression strength and compressive

modulus or stiffness. It would be ideal to match that of human bone. However, increasing the porosity decreases mechanical properties considerably. Therefore scaffolding options must always try to better mechanical properties as well as vascularity while maintaining the optimal balance. [73]

1.4 Current treatment options

The current treatments include autografts, allografts, material based grafts, distraction osteogenesis, bone lengthening, bone cement filters, BMP and distraction osteogenesis. [62, 78]

Grafting is required in orthopedic, oral and maxillofacial surgeries for skeletal reconstruction of long defects with no potential to self-heal caused by trauma, infection, tumor resection, skeletal abnormalities, compromised regenerative process in cases of avascular necrosis and osteoporosis. Here other options such as bone lengthening would not work. [61]

Autografts are hemocompatible, and non-immunogenic, but costly and cause donor site morbidity, as well as surgical risks. Another consideration with respect to autograft usage is the limited volume of harvestable iliac crest bone in skeletally immature patients (children). [7] Allografts are mostly hemocompatible and are available in different sizes as per patient requirement. However, there is shortage of supply and the concern of transmission of infections. The current material options are Biological materials (e.g. ECM), Xenografts (e.g. Bio-Oss/bovine bone granules), Natural polymers (collagen, fibrin, gelatin, silk), Bioceramics – Ca-P based apatites such as HA, synthetic apatites such as beta-TCP, HA/TCP composites, and bioactive glass. The other material based options are synthetic polymers - ester based such as PLGA, PCL, and PLLA and non-ester based such as PEG, PUV, and Silicone. [36] Xenografts have been shown to have good metabolic activity and ALP expression. The disadvantage however is at the decellularisation step where foreign cellular antigens can trigger an inflammatory response and/or tissue rejection. [36]

Polymers are preferred for scaffolding due to their strength, rate of degradation, porosity, shape, size, microarchitecture, attached to different functional groups easily to better offer an osteoconductive environment, and, easy and controllable reproducibility. [50] PLA or Poly-lactic acid is the synthetic biodegradable and biocompatible polymer used for fabrication of the scaffold in this project. PLA is a FDA-approved Generally Recognized as Safe (GRAS) polymer that is used in numerous resorbable surgical devices such as sutures, ligatures and meshes.

PLA is biodegradable because it can be cleared through the tricarboxylic acid cycle, as a medically innocuous lactic acid. [43] The possible disadvantages or challenges of using this material is the bulk erosion process they undergo which might lead to failure of the scaffold and abrupt acidic degradation products which then causes a strong inflammatory response. [43, 44, 45].

With respect to degradation rates, among the saturated polyesters, PLA degrades slower than PGA and PDLLA as it is more hydrophobic, but faster than PCL. Heterogeneous degradation takes place in thick scaffolds, i.e. degrades faster on the inside than on the outside due to neutralization of the carboxylic end groups on the PLA surface. In this case bulk erosion does not happen as acidity release is limited. In bulk erosion however, there is autocatalysis due to the carboxylic end groups which aren't neutralized. [43, 46] Thus, surface erosion is preferred over bulk erosion as it usually occurs at a constant rate. The more the crystallinity, the lesser and slower the bulk erosion and/or degradation. Upon implantation it might take up to 5 years for complete absorption of PLA. [43, 47]

HA is another material used in the whole scaffold, and is a CaP apatite that has been shown by the lab to improve mineralization and mechanical properties. [21] This is due to low grain size (nano), high crystallinity, and wet conditions – leads to higher stiffness, strength and fracture toughness. Increasing the porosity reduces the mechanical properties and fracture toughness [48], and further diminishes rapidly post implantation at a rate proportional to the in-vivo duration. [58]

Equivalence of synthetic grafts to allograft has been shown, with both in-vitro as well as clinical findings suggesting no statistically significant difference existed between the two to treat bony lesions. The only difference was the presence of cell remnants observed in the in-vitro testing of the allograft group, which could be related to risk of immunological response related to allograft usage. [6]

1.5 Rapid prototyping (RP) as scaffold technology

Fabrication techniques usually used in BTE include TIPS (Thermally Induced Phase Separation), LENS (heat laser metallic printing), RP (Rapid Prototyping) and electrospinning.

Different types of RP printing techniques are 3D printing or 3DP, Fused Deposition Modeling (FDM), 3D plotting, Selective Laser Sintering (SLS), etcetera. For the purposes of this project FFF/FDM i.e. Fused Filament Fabrication/Fused Deposition Modeling is used. The resolution is determined by nozzle size which dictates scaffold's microstructure design and porosity. Though 3D printing and came before FDM and are technically different, in today's language it refers to FDM.

In this method a controlled extruder is used to force out a filament material. This extruded filament material is deposited on a build plate platform where the design is fabricated layer by layer. The nozzle and the extruder are collectively called the 'print head'. The print head moves along the x-axis while the build plate moves along the Z axis. The Bowden tube leads the filament from the feeder to the print head. The feeder is connected to the printer's retraction setting, filament is withdrawn or retracted, for example when a pore has to be formed.

The FDM printer used for this project is called the Ultimaker 2+. The picture below highlights these features of the printer. The design file is saved in .stl format, and sliced using the software Cura, and saved as a gcode. This gcode is then used by the Ultimaker to print the design.

Fabrication using SLS doesn't require filaments which would be helpful in printing using new materials in different ratios without casting and extruding into filaments. However, pore sizes is

compromised as with SLS they are in the range of 1.75-2.5 mm as opposed to 200 µm fabricated using FDM. [29]

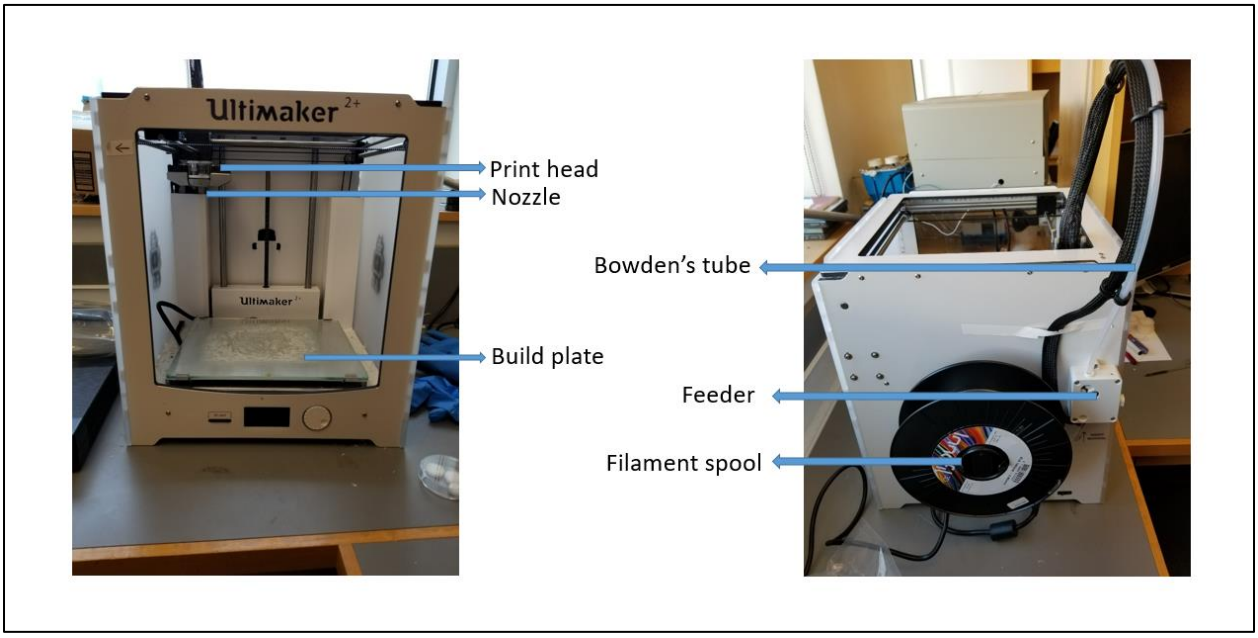

Figure 1: The 3D printer.

The advantages of using rapid prototyping for bone scaffolding are numerous. Scaffolds can be designed for one size and can be scaled up for big sized defects and scaled down for smaller defects. The printer can be installed in the operation room in hospitals or clinics to print scaffolds of exact dimensions during surgery.

Groups are using RP technology using a variety of materials including PLA. [79] The scaffold fabricated for this project has porosity and dimensional values that has a significant competitive advantage over existing scaffolds. [18]

Orthopedic medical devices fabricated using 3DP methods (additive manufacturing) have great potential due to enhanced biocompatibility, customizability, and cost effectiveness. [16] Other distinct advantages of using 3DP include easy fabrication of intricate surface textures and interior geometries with reduced material waste generation. The biggest concern when 3DP devices or scaffolds reach the manufacturing stage would be cleaning and sterilizing for incorporation into the body. [16]

Sterilization is usually a chemical (Ethylene oxide or supercritical CO2) or physical (UV, beta or gamma radiation) processes. [22] Autoclaving compromises structural integrity of PLA [23]. Gas sterilization using Ethylene oxide has disadvantages as models with porosities can trap the EO gas used for sterilization, and lead to problems after implantation. [16] PLA is extruded for 3DP in the range of 180-210 ˚C. Dry heat is recommended for materials with melting temperature less than 170 ˚C and steam sterilization for those less than 121 ˚C as PLA doesn't fit this criteria, these methods are ruled out. [24], [26] Soaking PLA scaffolds in glutaraldehyde (2.4% glutaraldehyde solution with a pH of 7.5) for 20 minutes at 25° C is suggested for sterilization. [24], [25].

The different possibilities with respect to sterilization are discussed in this white paper by Nelson Laboratories. It is highlighted that due to the complex internal and external geometries, sterilants might require more time to enter and exit the 3DP models. Models with porosities can trap the EO gas used for sterilization, and might require a higher aeration time. On the other hand, sterilizing a 3DP polymer model using radiation (gamma or electron beam) should also be carefully evaluated for unwanted crosslinking and curing leading to model configuration changes. Radiation sterilization is size and shape dependent, and even for the same polymer a 3DP version is incomparable to a milled/molded version. [16] 3DP with metal oxide leads to micro-void formation which leads to reduced biocompatibility and safety. SLS printing with the same might lead to some metal oxide sacrificial support unremoved from device before implantation which could have toxic effects in the patient's body. [16]

1.6 Aim of the Project

The aim of the project was to use rapid prototyping technology to develop biocompatible, osteoinductive, osteoconductive, highly porous and pre-vascularized bone scaffolds with desirable mechanical properties. The lab previously came up with the idea of fabricating cortical part of the scaffold by mimicking the structure of the osteon, and this was done by electrospinning technique. In this project, I design the scaffold to improve porosity and load bearing capabilities, and fabricate it using rapid prototyping technology. The cortical part of the scaffolds are pre-vascularized, and the cell studies are focused on achieving bone growth in the trabecular portion on the scaffold, and vascular growth in the cortical portion of the scaffold.

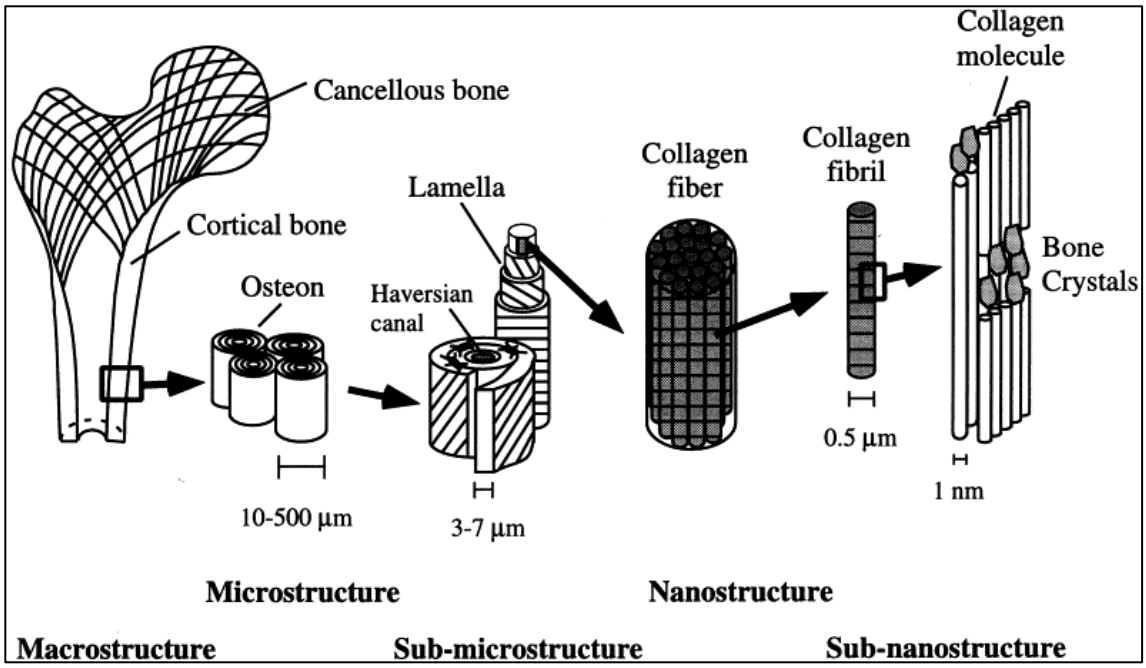

Figure 2: Bone macro, micro and nanostructure from J. –Y. Rho et al [73], used with permission.

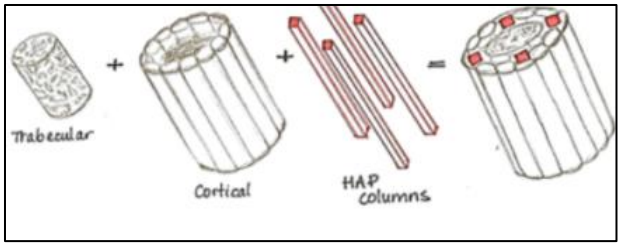

Figure 3: Designing cortical of whole bone scaffold by mimicking the structure of bone osteon and mechanically reinforcing with hydroxyapatite columns. [71], [74]

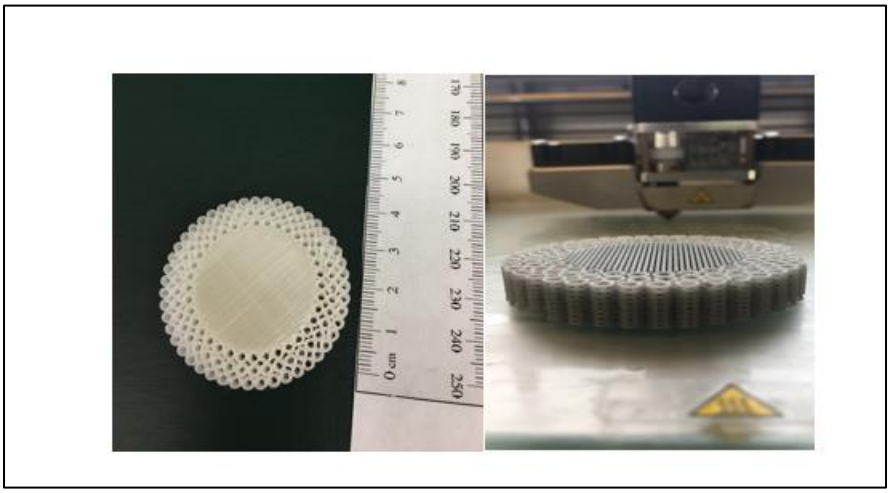

Figure 4: 3D printed scaffolds for bone regeneration, highly porous, load bearing and scalable.

CHAPTER 2-Scaffold Fabrication and Characterization of Scaffold Structure, Mechanical Properties and Cell Biocompatibility

2.1 Evolution of design and prototyping of scaffolds

Design ideas were implemented using Solidworks before selecting the final design. The design decisions were driven by the need to maximize the number of pores while maintaining structural integrity of the scaffold. The first design draft had a single layer of central mesh extruded to the required height to represent the trabecular bone. It had side circles with gaps present that represented the cortical part of the bone. A few side circles were shaped with smaller diameters to host hydroxyapatite posts. This design is called 'D1M1' (Design 1, Mesh 1). This can be observed in the figure 5 below. The square holes in the trabecular region were 0.9mmx0.9mm.

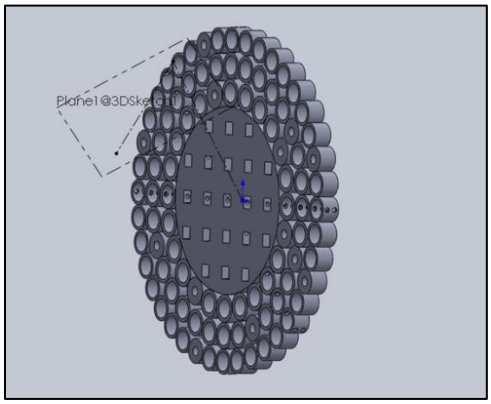

Figure 5: Representation of Design 1(D1M1)

This design was improved upon by increasing the frequency of pores on the mesh/trabecular region, as well as creating multiple layers of mesh separated and supported by solid columns, and called 'M2'.The idea was to facilitate movement of cells, oxygen and nutrients within and through the scaffold. The cortical portion is kept the same as in D1M1.The new mesh and the layer separation can be observed below in figure 6. This design is called 'D1M2' (Design 1, mesh 2).

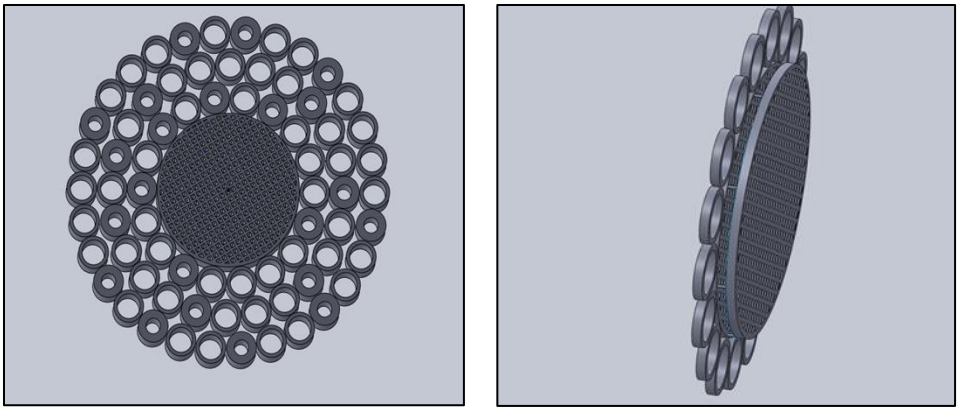

Figure 6: Representation of D1M2, with emphasis on increased number of gaps and the layer separators.

However this design cannot hold, as the mechanical properties would not be favorable with small columns supporting the entire number of layers of the trabecular/mesh region.

Another design idea was to fashion a two piece elliptical shaped scaffolds- the two pieces can then be joined together to get one scaffold. Both pieces resembled the mesh portion described in previous design (M2). This would ensure separate scaffolds that might be useful during cell studies, wherein the cortical scaffold can be vascularized and the trabecular portion can then be added to the pre-vascularized cortical portion. After being combined, the whole scaffold can be seeded with HMSCs to induce bone formation. This kind of design has good utility. This design can be seen in the Figure 7 below, and is called D2 (i.e. Design 2). The square holes in the trabecular region of M2 were 0.9mmx0.9mm. The hollow cortical was 2mm in radius, while the cortical sides for post had a thickness of 0.8mm.

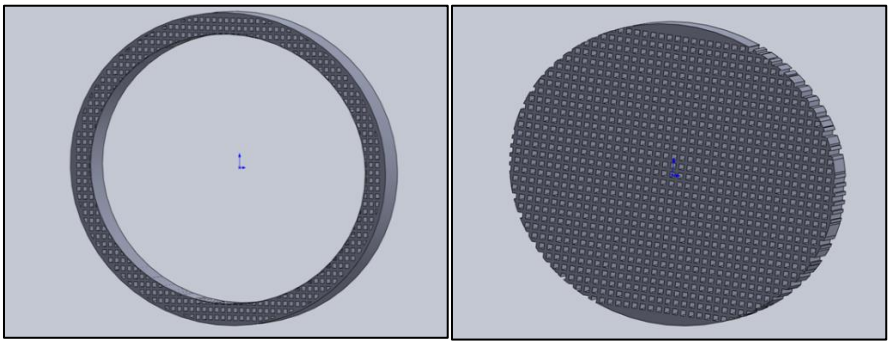

Figure 7: D2M1 (Design 2, Mesh 1), cortical (outside) and trabecular (inside) portion of the scaffold.

The next design, D3 (with Mesh 1 as well as Mesh 2) had the same trabecular mesh portion, but different cortical design, as can be seen in figure 8. This design was to have a division within the cortical portion so as to have multiple/alternate flow paths to facilitate movement. But it wasn't printed as it did not address a lot of issues like mechanical integrity in the presence of a load, porosity and didn't seem like it would serve as a sheltered base to help in the attachment and proliferation of vascular cells as required. There would not really be any control in the kind of cells/fluids that could flow through, or the rate of flow, or the formation of blood vessels in a preferred direction.

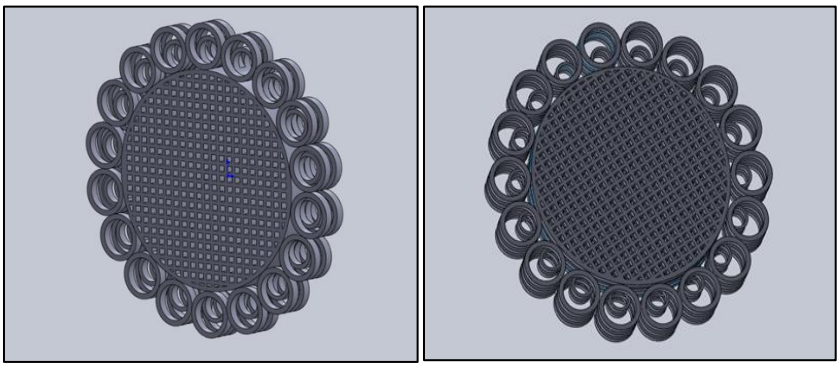

Figure 8: D3M1 (left) and D3M2 (right)

To overcome the shortcomings of the previous designs, the final design incorporates a 5 layer mesh that it laid horizontally and vertically, alternatingly, thus creating a cross-section mesh (M3). This mesh works upon the M1, but also increases pores on the side - M1 did not have any outlets on its side. Unlike M2 the layers aren't supported by columns. Therefore, higher porosity, better mechanical integrity, and horizontal as well as vertical flow paths is achieved. This can be observed in the Figure 9 below. The overall dimension for D2 was 9.75mmx9.195mmx5mm (outside) and 4.5mmx3.9mmx5mm (inside) after scaling down by 50% and printing.

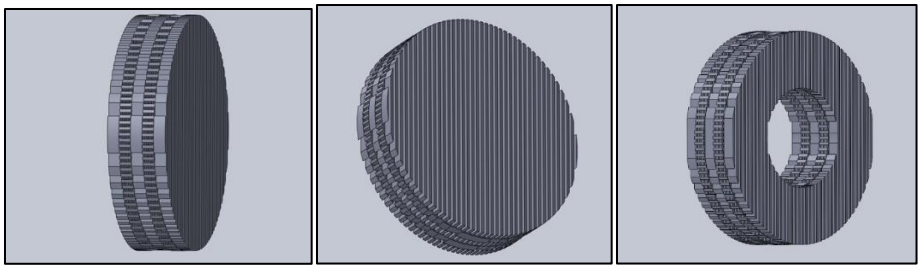

Figure 9: M3 side view (left), M3 front view (middle), D2M3 ‘outside’ (right).

This mesh (M3) forms the trabecular portion of the scaffold. The cortical section forms layers around the circular outline of the trabecular portion. It has long hollow cylindrical structures with pores on its walls. The hollow cortical portions allow incorporation of hydroxyapatite posts as required to enable better mechanical strength in vivo. The cortical side circles all have the same diameters so any or all of them can be filled with hydroxyapatite columns as required. This final design is called D4M3 (Design 4, Mesh 3) and can be seen in the figure 10 below. The design specifications for this design are spacing between mesh struts 0.5mm, length of longest vertical strut 0.0331701m, length of longest horizontal strut 0.03312608m, cortical diameter of 1mm, cortical side pores 300µm).

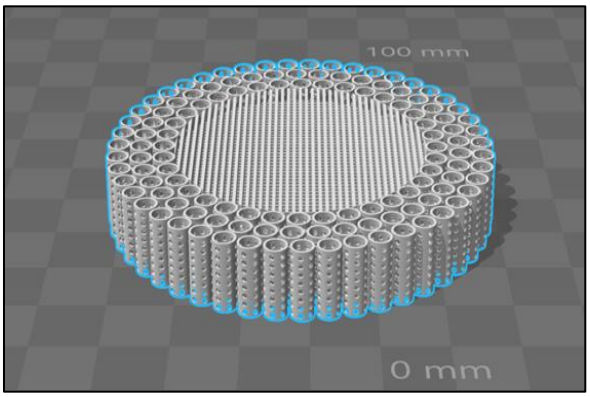

Figure 10: Schematic of D4M3, the final design.

Throughout the designing process the spacing of the mesh struts (horizontal and vertical columns) were altered to maximize porosity. Cura was the software used for scaling and slicing the designs, which then generates the gcode. The gcode was then uploaded on to the 3D printer to begin printing, after the printing properties were suitably adjusted.

2.2 Materials and Methods

PLA (Gizmo Dorks) is a commonly used thermoplastic polymer for additive manufacturing and was selected because it's prior FDA approval, biocompatibility, easy handling, availability and fabrication, and required biodegradation duration. PLA scaffolds were printed using an Ultimaker 2+ 3D printer. They were designed using Solidworks (Dassault System) with emphasis on porosity and pore size, and sliced using Cura Software.

2.2.1 Fabrication of scaffolds using PLA

The designs were 3D printed with PLA obtained from Amazon (clear/transparent or silver PLA). The silver PLA was used till final design good quality print was achieved, post which scaffolds for cell studies were printed using clear/transparent PLA.

The parameters for printing with PLA used were - nozzle temperature 180-210 ˚C, the build plate temperature of 45-60 ˚C (altered according to print), and the material flow rate at 100%, brim and initial layer speed at 30%, fan speed adjusted per print from 0-100%. The resolution is determined by nozzle size which dictates scaffold's microstructure design and porosity. The nozzle size used for this project was 0.25mm.

2.2.2 Fabrication of scaffolds using materials other than PLA

An attempt was made to use PLLA as a filament material as well as a 1:1 PLA and hydroxyapatite (HAp) filament. This would lead to using home-made filaments and provide flexibility to use different compositions. A (7% w/v) PLLA was made using PLLA (MW = 152,000, Sigma Aldrich, St. Louis, MO, USA), Dichloromethane or DCM (Sigma Aldrich, St. Louis, MO) and Dimethylformamide or DMF (Sigma Aldrich, St. Louis, MO). In the case of 1:1 PLA and HAp, PLA pieces (from the PLA filaments) and HAp (Synthetic nanopowder, <100nm, Sigma Aldrich, St. Louis, MO, USA) were mixed with 3.4mL of Tetrahydrofuran or THF (Sigma Aldrich, St. Louis, MO) (3.4mL/g total) and Dimethylformamide or DMF (1.1 mL/g). The

magnetic stirrer of appropriate size was put into the beaker, sealed with white tape and parafilm to prevent solvent evaporation, and placed on a magnetic plate. The next day the parafilm was removed along with the magnet. The solution was cast on Bytac sheet and left undisturbed for 3 days post which it was cut into small pieces and extruded using the Wellzoom extruder. The solutes used in the simulated body fluid (SBF), sodium chloride (NaCl), potassium chloride (KCl), calcium chloride dihydrate ($CaCl.H_20$), magnesium chloride heptahydrate (MgCl2.H20), sodium bicarbonate ($NaHCO_3$), and sodium phosphate monobasic(NaH_2PO4) were purchased from Fisher Scientific (Pittsburgh, PA, USA).

2.2.3 Pore formation

As mentioned in the introduction section, there must be presence of macro as well as micro pores on scaffolds for premium functioning. This is done in three ways on the scaffold. The first is by designing the mesh/trabecular portion of the scaffold with required strut spacing, and designing pores on the sides of the cortical part of the scaffold. Thus, pores in the range preferred by osteoblasts were introduced by virtue of design in the trabecular region. Micro pores and macro pores were introduced by soak-freeze method. This involved soaking scaffolds in DI water for an hour, and changing water after 30 minutes. The water was removed, post which the scaffolds were frozen by placing in the freezer overnight. Initially, the scaffolds were placed in -80 ˚C overnight. Later, experiments were carried out by placing scaffold in -20 ˚C overnight, -80 ˚C overnight and in liquid nitrogen and it was found that the optimal sequence would be freezing in -20 ˚C overnight as well as freezing in -80 ˚C overnight. A pure mesh scaffold with 4.5mm (long radius), 3.9mm (short radius), and extrusion height of 5mm was used as seen in Figure 11 below. Scanning Electron Microscopy or SEM was used to obtain pictures of scaffolds subjected to the soak freeze technique and scaffolds not subjected to the soak-freeze. This was done to check for presence and structure of soak-freeze induced pores, presence of designed gaps in the mesh/trabecular region, and check the effect of soaking before freezing.

The LEP -1100A Liquid Extrusion Porosimeter (PMI, Ithaca, NY) was used to check the range of pore sizes introduced in scaffolds when they were soaked for an hour in DI water and kept overnight in -20 degrees Celsius, -80 degrees Celsius and Liquid Nitrogen respectively.

2.2.4 Mineralization

Mineralization is the process by which calcium ions from simulated body fluid (SBF) attach to the nucleation sites within the scaffold. SBF has calcium concentration similar to blood plasma, and the addition of the inorganic content in the form of Ca ions improves the scaffold's structural integrity and osteoblastic differentiation. [19] Mineralization is done to improve bone formation. Static mineralization was carried out in 10 X SBF, and the scaffolds for sequential treatment, degradation studies and cell studies were mineralized in this manner. The ingredients for SBF. The mineralization procedure followed involved placing scaffolds in vials filled with 100:1 SBF and $NaHCO_3$ (17mL of SBF and 170 µL of $NaHCO_3$) and placing the vials on a shaker. [20] For sequential studies as well as the preliminary cell studies, involving rat fibroblasts and HMECs respectively, mineralization was carried out for 3 hours, with solution being changed after 1 hour. For the final cell study involving HMECs and HMSCs, as well as the whole scaffold compression testing, mineralization was done for 10 hours with solution being changed after 1 hour. This was done after tests showed mineral content is higher for scaffolds in 10 X SBF for 10 hours, beyond which there is no further increase. It has also been shown by the lab previously that higher level of minerals in the inside of scaffolds are seen for longer mineralization durations. [19]

2.2.5 List of sequential pre-treatments

The final scaffold has to have high porosity, good mechanical strength and support bone formation. Three pre-treatments were tried in different sequences, namely, soak-freeze, mineralization and NaOH treatment to best judge which treatments are preferable. The Sodium hydroxide pellets are from Fisher Scientific (Pittsburg, PA, USA). There are 8 batches based on the sequence of these treatments. All batches were ultimately tested with respect to compression

(n=4), ash weights (n=3) and Alizarin Staining (n=3). The batches were – B1 - 'Control (no processing)', B2 - 'Only Mineralise', B3 - 'NaOH+ Mineralise', B4 - 'Only NaOH', B5 - 'Only soak-freeze', B6 - 'Soak-freeze+Mineralise', B7 -'Soak-freeze+NaOH+Mineralise' and B8 - 'Soak-freeze+NaOH'. Scaffolds in batches 3, 4, 7 and 8, were soaked in 0.1 M NaOH solution for 5 minutes in vacuum, and then rinsed in DI water. The samples were then placed in 10xSBF on a shaker for 3 hours, with solution being changed every hour, rinsed with DI water and preserved in the desiccator [21] Soak-freeze involved soaking the scaffold for 1 hour in DI water, changing water after half an hour, removing the scaffold from water and placing it in the -80 ˚C overnight. Mineralization was done as mentioned in the previous section 2.4).

Batches
B1 - No processing
B2 - Mineralize
B3 - NaOH, Mineralize
B4 - NaOH
B5 - Soak-freeze
B6 - Soak-Freeze, Mineralize
B7 - Soak-Freeze, NaOH, Mineralize
B8 - Soak-Freeze, NaOH

Table1: Batches highlighting different sequential pre-treatments tested on scaffolds.

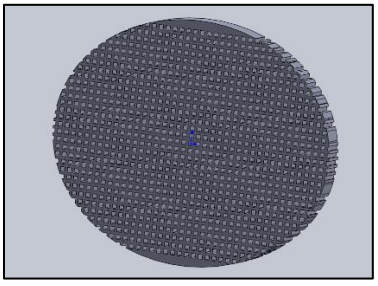

Figure 11: Design of scaffold used for sequential pre-treatments and porosimeter testing.

2.2.6 Mechanical Characterization

The Instron 5869 was used to test the scaffolds in compression until failure with a uniform strain rate of 1 mm per minute. The data generated was analyzed to determine the yield stress, compressive modulus and ultimate compression strength. During the sequence test, a pure mesh scaffold with 4.5mm (long radius), 3.9mm (short radius), and extrusion height of 5mm was used. Compression testing was done on whole scaffold (radius 12.88 mm, height 8.1mm and distance between struts 0.5 mm.) that was not soak–frozen and mineralized (n=1). Compression testing was also carried out on scaffolds that were soak-frozen overnight, and then mineralized for 10 hours (n=4). These latter scaffolds had two HAP posts inserted into the cortical. HAP has previously been shown by our group to increase mechanical properties of scaffolds, and also contribute towards increased bioactivity and mineral precipitation on scaffold. [19]

2.2.7 Alizarin Red Staining

Mineral deposition was characterized using Alizarin red stain (Alizarin red powder, Sigma Aldrich). Scaffolds were first washed with PBS (Corning, Cellgro) once, then DI water. Then they were incubated with a 40 mM Alizarin red solution for 10 minutes. The scaffolds were then washed five times with DI water. They were then washed once with PBS, and incubated with PBS for 15 minutes. PBS is removed, and Cetylpyridinium chloride or CPC (Sigma Aldrich) is added to the scaffolds. Stain controls were made using CPC and Alizarin red stain, with a decreasing concentration curve 4mM, 1mM, 0.25mM, 0.025mM,0.0025 mM, 0.00025 mM, and 0.000025mM. 100 µL triplicates is removed from standards as well as scaffolds and put in a 96-well plate. Infinite M200 Pro plate reader and Icontrol software is used to read the plate at 652 nm and display absorbance.

2.2.8 Sterilization of Scaffolds

Scaffolds were subjected to sterilization before seeding. They were soaked in Glutaraldehyde (2.4% glutaraldehyde solution with a pH of 7.5) followed by 30 minutes under UV light was used

for the initial cell study with rat fibroblasts. [24], [25]. For the following cell studies the samples were sterilized in 70% ethanol (Decon Labs) for 30 minutes followed by exposure to UV light for 30 minutes. [21]

2.2.9 Cell Seeding (Rat Fibroblasts, HMECs, HMSCs)

In the initial phase of the project, scaffold (1mmx1mmx1mm) was seeded with rat fibroblasts from ATCC to check for biocompatibility and cell adherence. The scaffolds are sterilized and mineralized before seeding. The seeding density was 20,000 cells per cm square. The media used for this study was α-MEM (Life Technologies, Grand Island, NY, USA) with 10% Fetal Bovine Serum or FBS (Sigma Aldrich, Atlanta, Georgia) and 1% Penicillin-Streptomycin (Sigma Aldrich, Atlanta, Georgia). Presto blue (Thermo Fisher Scientific) assay was conducted on days 3 and 7. Imaging was done staining for DAPI and Phalloidin (Thermo Fisher Scientific).

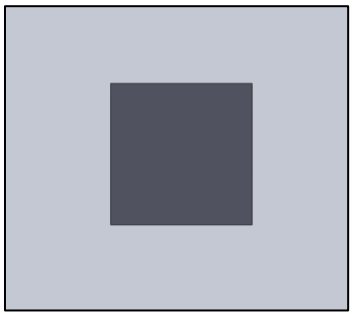

Figure 12: Design of a simple scaffold used to check for biocompatibility.

As mentioned in the introduction, the experimental plan was to pre-vascularize the cortical sections of the scaffolds by seeding them with Human Mammary Epithelial Cells or HMECs (ATCC). A preliminary 21 day cell study was thus done using HMECs on scaffolds (trabecular diameter as 10.6mm, cortical diameter as 1mm and extrusion of 5mm, n=4) as shown in figure 13 below. Before seeding, the scaffolds are mineralized. Before they are mineralized, the cortical sections are filled with alginate (8% wt) and crosslinked with 0.1M Calcium chloride solution to block mineralization in the cortical sections. The media used for this study was MCDB131 (Life Technologies) with 1µg/mL hydrocortisone, 10mM glutamine, 10% FBS, 1% Penicillin-

Streptomycin, and epidermal growth factor or EGF (10ng/mL). For the preliminary cell study the scaffolds were seeded at P4 with a high seeding density of >100,000 cells per cm square.

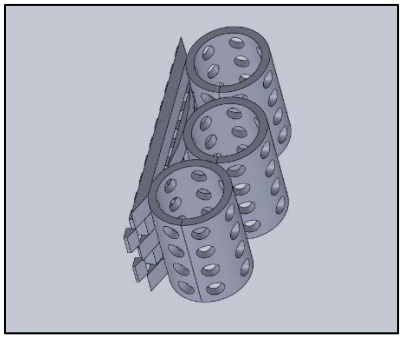

Figure 13: Design of scaffold used for HMEC+HMSC study.

The final HMECs cell study was a 14 day study with scaffolds (trabecular diameter as 10.6mm, cortical diameter as 1mm and extrusion of 5mm, n=30) seeded at P5 with a seeding density of 50,000 cells per cm square. The same procedure outlined for the preliminary HMEC cell study was followed. Scaffolds (n=4) and TCP were fixed using 4% Paraformaldehyde or PFA (Sigma Aldrich, St. Louis, MO, USA) for CD31 staining. The remaining scaffolds were decellularised by following a protocol the lab came up with previously which involves placing the scaffolds in liquid nitrogen and water bath, in that sequence followed by washing scaffolds with PBS. This is done thrice (3x). The scaffolds are then placed in -80 ˚C freezer till the scaffolds will be used for the HMSC cell study.

The final Human bone marrow derived Mesenchymal Stem Cells or HMSC (ATCC) study was for a duration of 12 days. It had two groups of scaffolds, the pre-vascularized and decellularised scaffolds from the HMEC study, and fresh non-vascularized mineralized scaffolds. Both the scaffolds were sterilized as mentioned in 2.7. The scaffolds were seeded with cells at P3 and a seeding density of 15,000 cells per cm square.

HMSCs were grown in osteogenic media - the Mesenchymal Stem Cell Growth kit, with Mesenchymal Stem Cell Basal Medium Medium, L-Alanyl-L-Glutamine, 30% FBS, rh-IGF, rh-FGF, 1% Penicillin-Streptomycin. (ATCC).

This is done to support the cells in establishing an osteoblast like phenotype. During seeding on scaffolds as well as subsequent feeding the media used was standard osteoblast media without any osteogenic factors - α-MEM (Life Technologies) with 10% Fetal Bovine Serum or FBS and 1% Penicillin-Streptomycin. Scaffolds (n=8) and TCP from were fixed on Days 4, 8 and 12. This was done for ALP and CD31 imaging. ALP kit was purchased from Sigma-Aldrich. CD31 primary monoclonal antibody and secondary Alexa Flour were purchased from Thermo Fisher Scientific). All the images were obtained using Zeiss Microscope.

2.2.10 Degradation study

A degradation study was run for a duration of 8 weeks as PLA is known to show bulk degradation.

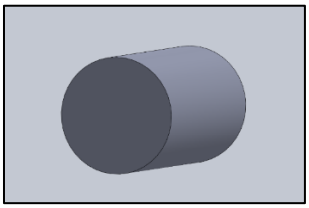

Figure 14: Scaffold used for degradation study.

Scaffolds (2mm radius and extrusion of 5mm, n=4 per time point) printed with PLA were placed in vials filled with 10 mL of phosphate-buffered saline (PBS) (pH 7.4). These vials were incubated in vitro using a shaker at 37 ˚C for a duration of 8 weeks. The PBS solution was replaced once a week. At specific time points – after week 0, after week 1, after week 4 and after 8 weeks - the scaffolds were removed and rinsed with DI water and tested for mineralization (Alizarin staining) and compression properties.

2.2.11 Statistical Analysis of Data

All the data was reported as Mean + Standard deviation. One-way analysis of variance (ANOVA) was used to determine if the differences between the groups were significant. A p value<0.05 was considered to be significant.

2. 3 Results and Discussion

2.3.1 Design and Printing of Scaffolds

The required designs and pore ranges were successfully produced and printed.

The initial designs were printed using silver/grey filament of PLA. Once the final designs were locked down, transparent/ natural/ clear PLA was used. This translucent property combined with the presence of pores enables easy procurement of better microscopic images. The duration for printing each design varies based on the complexity and size of the design, and, the speed of printing. The D2M3 pieces were printed in 45 minutes whereas the D4M3 was printed in 9 hours. This was because the print speed was kept low for the entire print duration to maximize quality and ensure good pore formation on the side of cortical portion. For designs of less complexity speed can be increased from 30% (initial layer) to 80-100%, and therefore reduce duration per print. Additionally, to get better quality prints, the ideas were designed in larger dimensions and scaled down by 20-30% on the Cura software, before the software sliced it to generate a gcode.

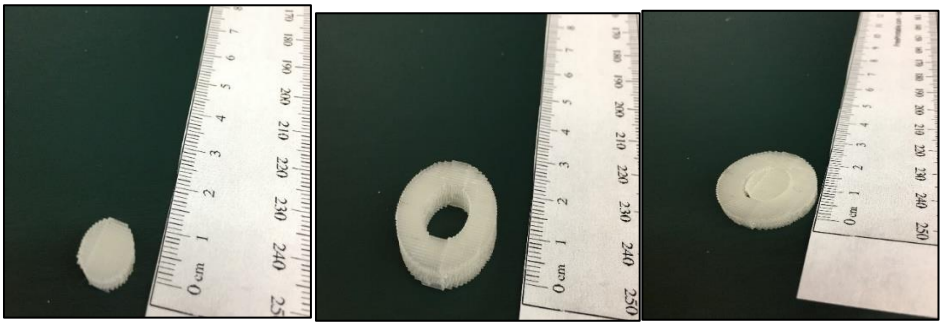

Figure 15: Printed cortical (left most) inner and trabecular outer (middle) sections and the complete (right most) ‘D2M3’ bone scaffold.

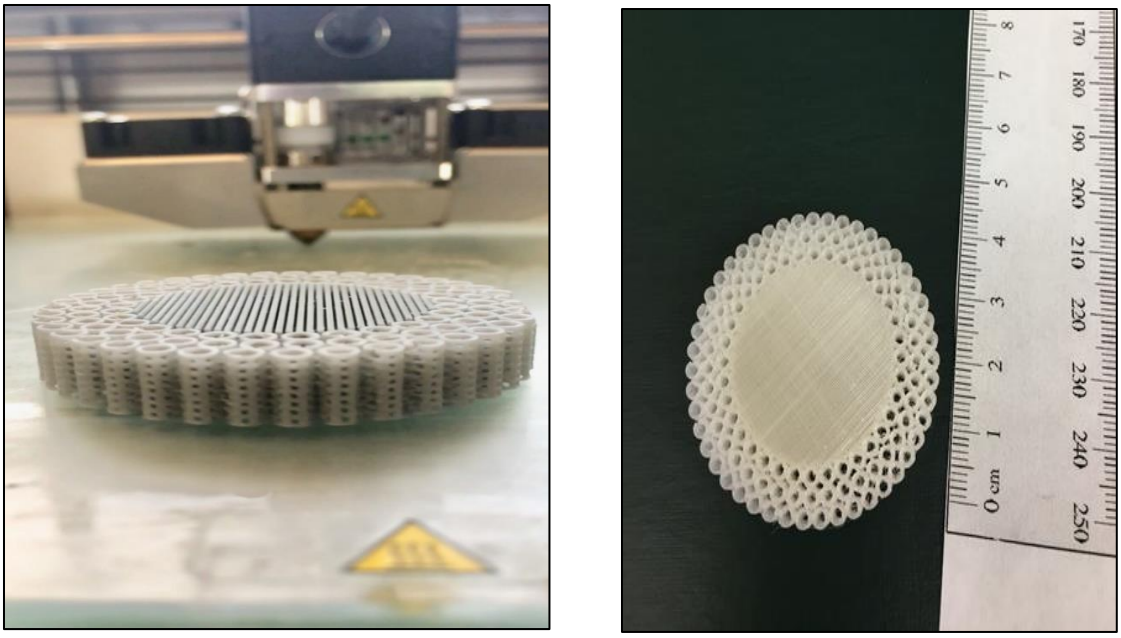

Figure 16: A picture of the final design D3M4 printed scaffold with emphasis on the pores present on the cortical section.

2.3.2 Pore formation

Pore presence, structure and distribution was observed using SEM and porosimeter. Using SEM it was possible to verify that the gaps between the struts in the trabecular/mesh region were printed and in the range of 300-350 µm as desired for osteoblast growth. This can be visualized in Figure 17. A clear difference was seen between scaffolds that were soaked before freezing and scaffolds that weren't soaked – there were no pores observed in the scaffolds that weren't soaked in water. This can be observed in Figure 18.

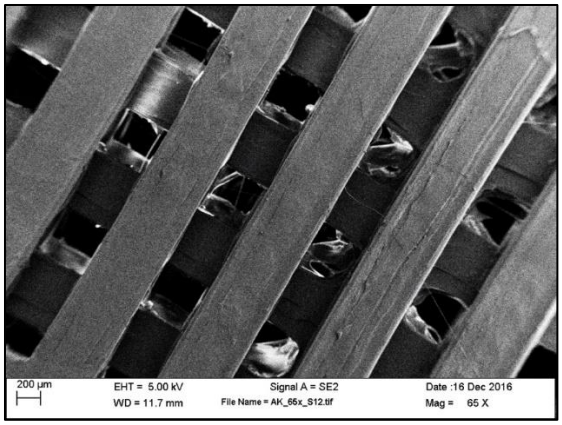

Figure 17: SEM image (65x), non-soak, frozen at -80 ˚C, no induced pores observed.

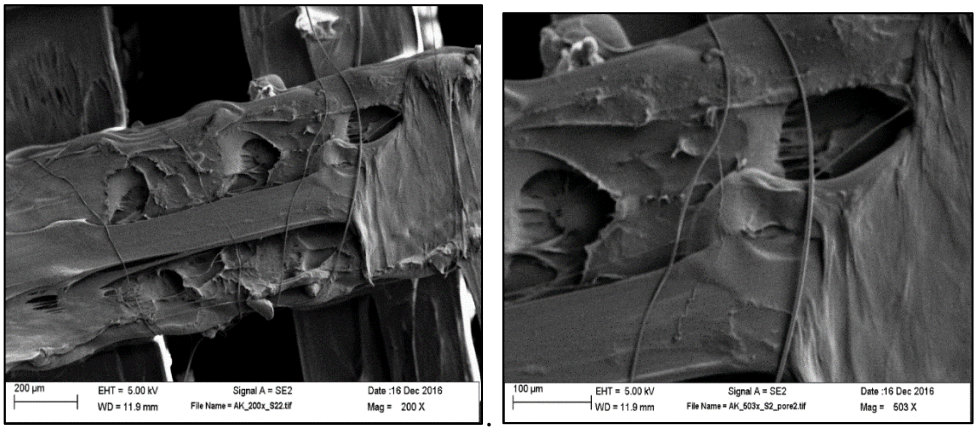

Figure 18: SEM image (left image at 200x), (right image at 503x) water soak, frozen at -80 ˚C, induced pores observed.

The data from the porosimeter seen in Figure 19, showed that scaffolds that were soaked and placed liquid nitrogen produced a high number of pores in 3000-4000 µm range.

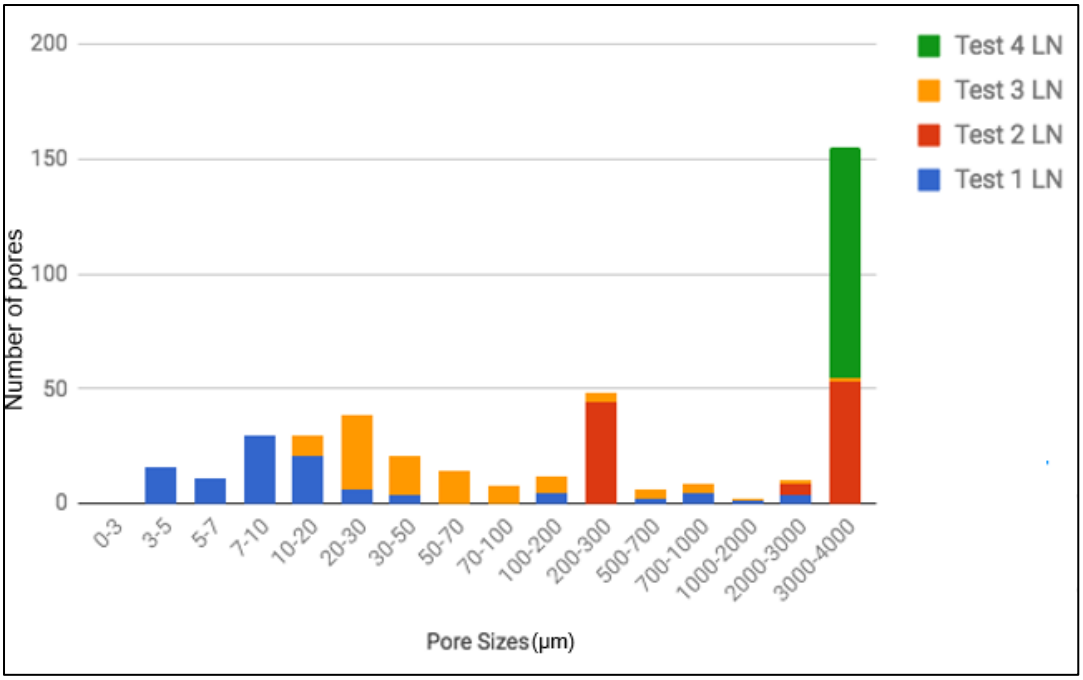

Figure 19: Pore sizes obtained when scaffolds soaked in water and dipped in Liquid Nitrogen.

Scaffolds that were soaked and placed in -20 ˚C also show a similar trend with higher number of pores being formed in the range of 3000-4000 µm, as can be seen in figure 20 below.

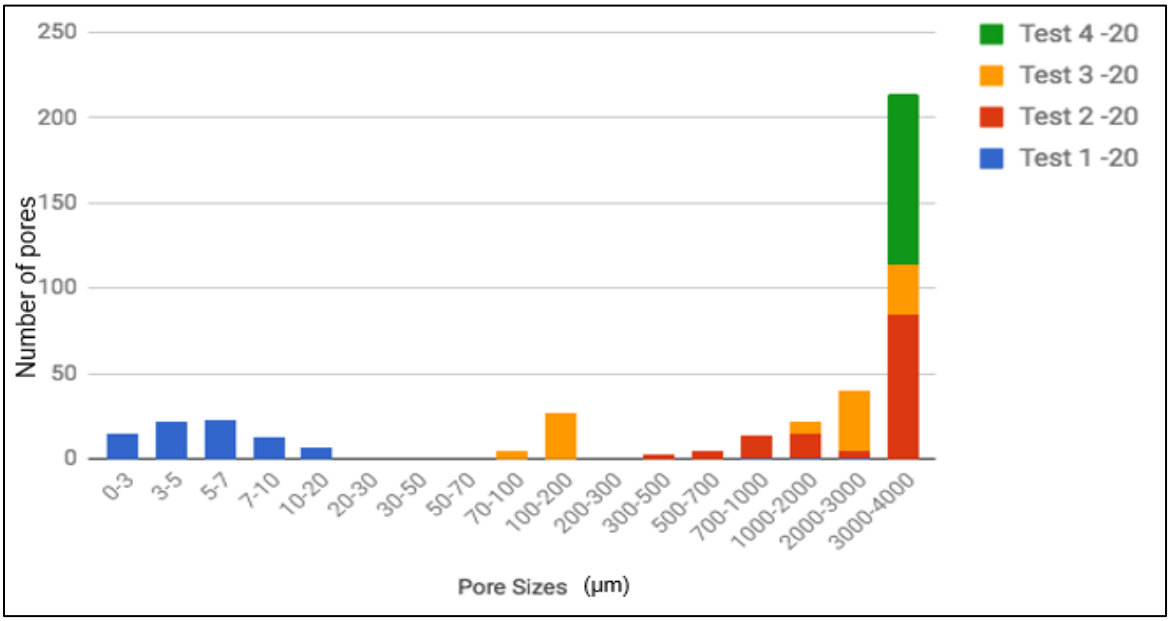

Figure 20: Pore sizes obtained when scaffolds soaked in water and placed in -20 freezer.

However, the difference between liquid nitrogen and -20 ˚C lies in the fact that there are almost no intermediate sized pores formed in -20 ˚C. This is a desirable feature for this project, and coupled with the observation that the number of pores formed in -20 ˚C is higher than liquid nitrogen, helps us choose -20 ˚C.

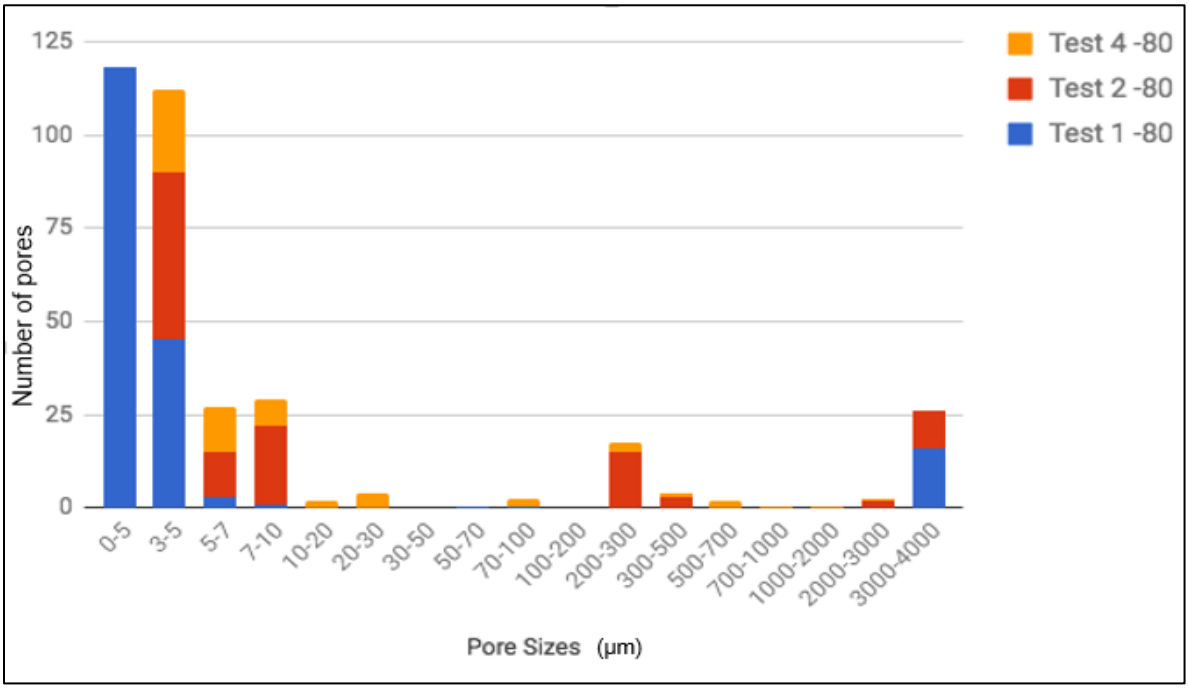

Figure 21: Pore sizes obtained when scaffolds soaked in water and placed in -80 freezer.

As seen in figure 21 above, scaffolds soaked and placed in -80 ˚C induced higher number of pores of about 5 µm which is favorable for vascularization.

Thus, -20 ˚C as well as -80 ˚C together yielded the best case scenario of achieving micro-pores as well as macro-pores. This was thus incorporated in the pre-treatment before the final cell seeding with HMECs and HMSCs. Thus scaffolds were soaked in water, frozen in -20 ˚C, followed by -80 ˚C, and then mineralized and sterilized before cell studies.

2.3.3 Alizarin red staining

The presence and concentration of the mineral was estimated by checking the sample's absorbance at 652 nm using an assay plate reader. The standard curve obtained is used to convert the absorbance values into concentration.

For the sequence test, the following data was gathered (Figure 22) which shows that, batches 3, 2 and 6 (in that order) corresponding to 'NaOH and Mineralize', 'Mineralize' and 'Soak-freeze and Mineralize' have the highest concentration/mineral retention. Considering the importance of pore formation by soak-freeze method, Batch 6 will thus be the preferred method with respect to mineralization.

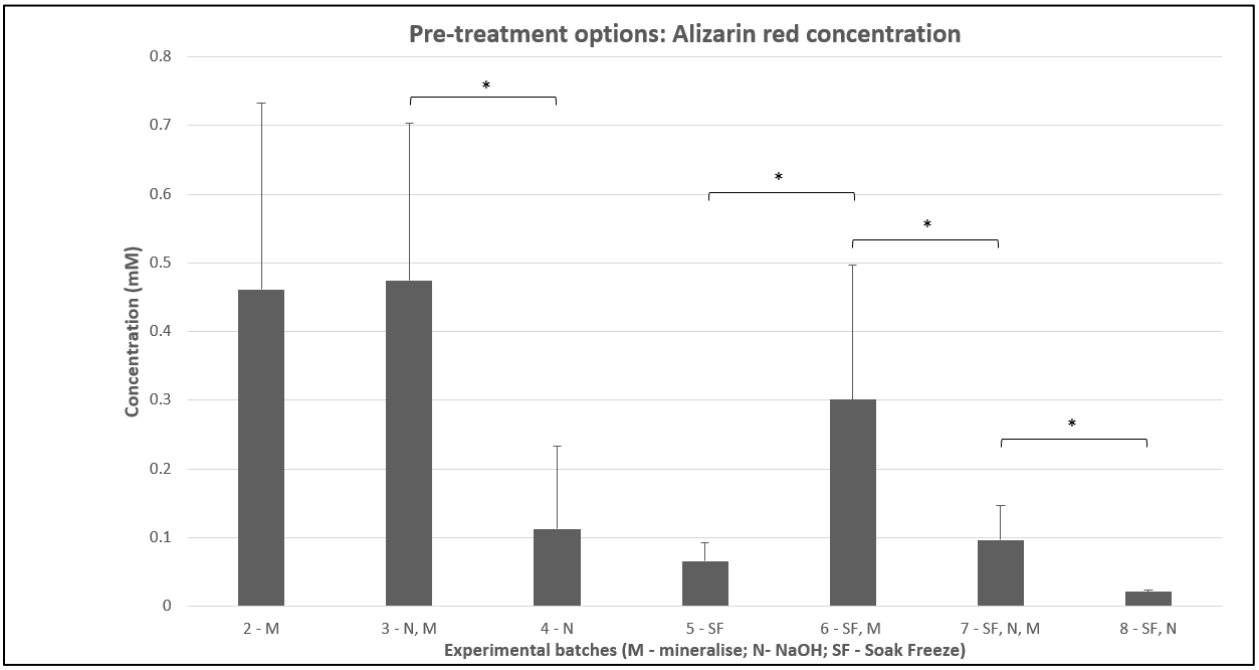

Figure 22: Alizarin concentration for the different experimental groups. The * denotes that the difference is statistically significant.

For the degradation test, the following data was obtained (Figure 23), which shows that there is good mineral retention for the first three time points with no significant difference, and will definitely support bone formation in the scaffolds.

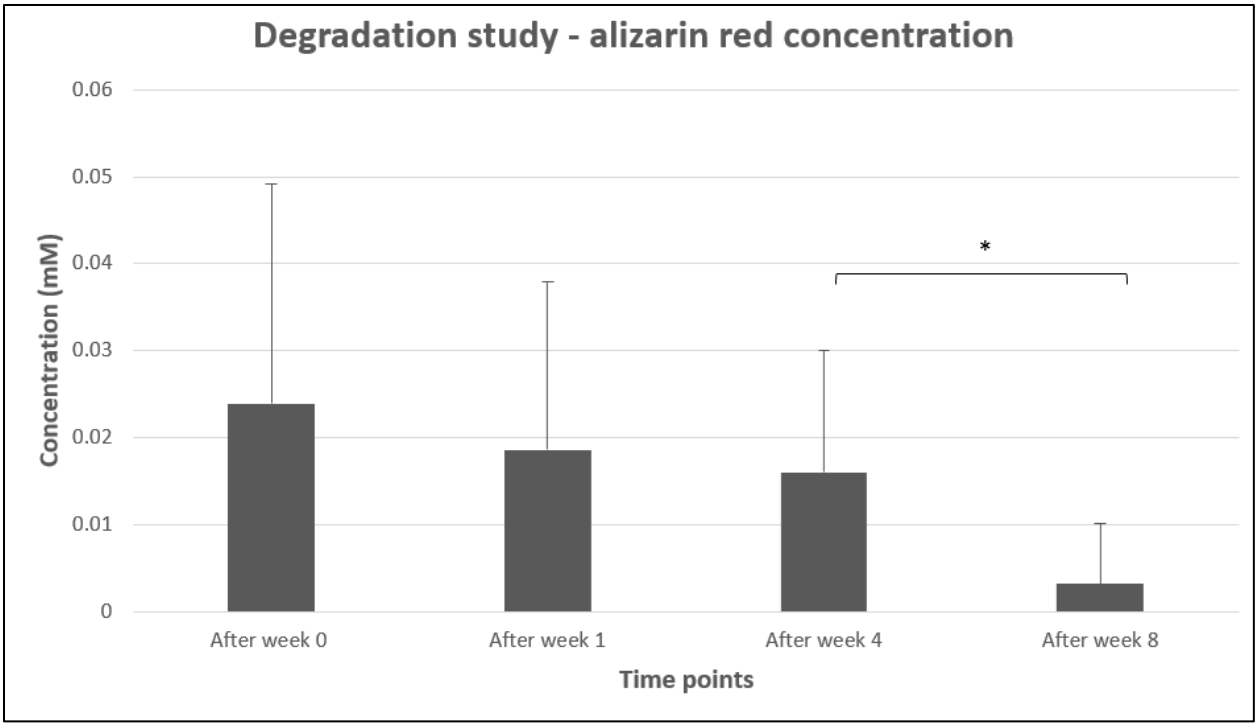

Figure 23: Alizarin concentration for the different time points in the degradation study. The * denotes that the difference is statistically significant.

2.3.4 Mechanical (Compression) Properties

The compression testing data on the different batches was done to determine the best pre-treatment option. There was no significant difference between the batches. Each parameter suggests different batches, however, the selection has to bear in mind that mineralization is a requirement (for bone formation) as is soak-freeze (for desirable additional porosity). In the whole bone scaffold, there is also the addition of hydroxyapatite posts to reinforce the scaffold mechanically. Keeping this in mind, it is clear that the selection is to be done between batches 5-8. After considering data from Alizarin testing to this decision making process, is was decided that Batch 6 is the preferred pre-treatment. It can be seen in the graph below that batch 6 has very good mechanical strength more than almost all options, and stiffness (modulus) comparable to cancellous bone. Batch 6 has a modulus of 0.714±0.142 GPa, as seen below.

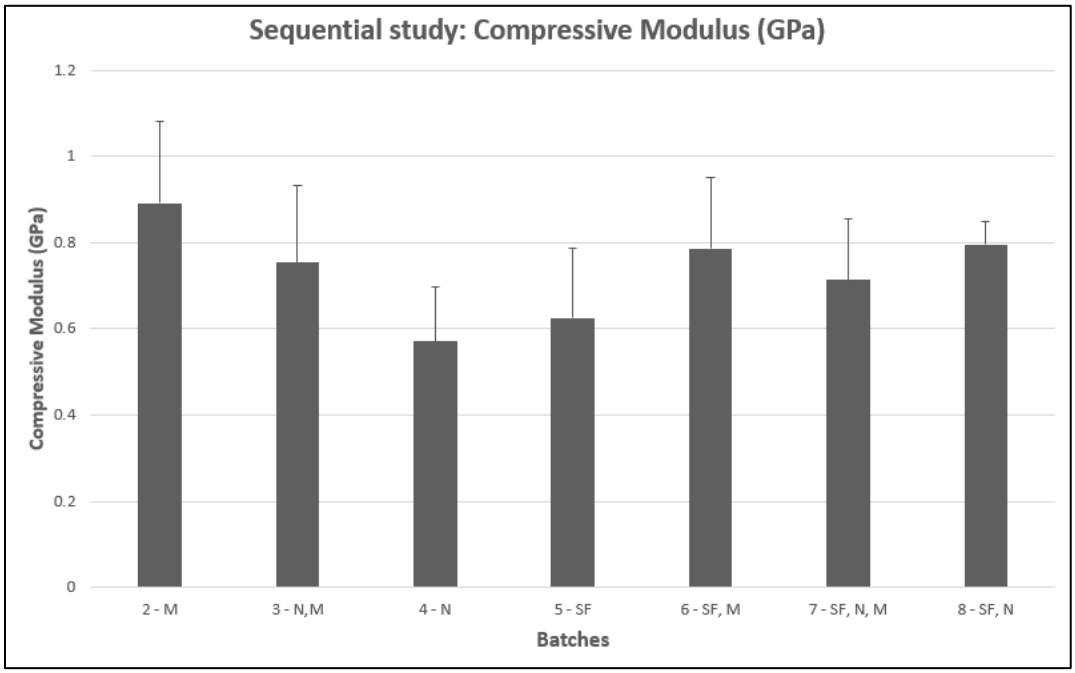

Figure 24: Compressive modulus of different experimental batches (GPa).

It can be seen in Figure 25 below that the ultimate compressive strength of batch 6 is 255.541±108.693 MPa.

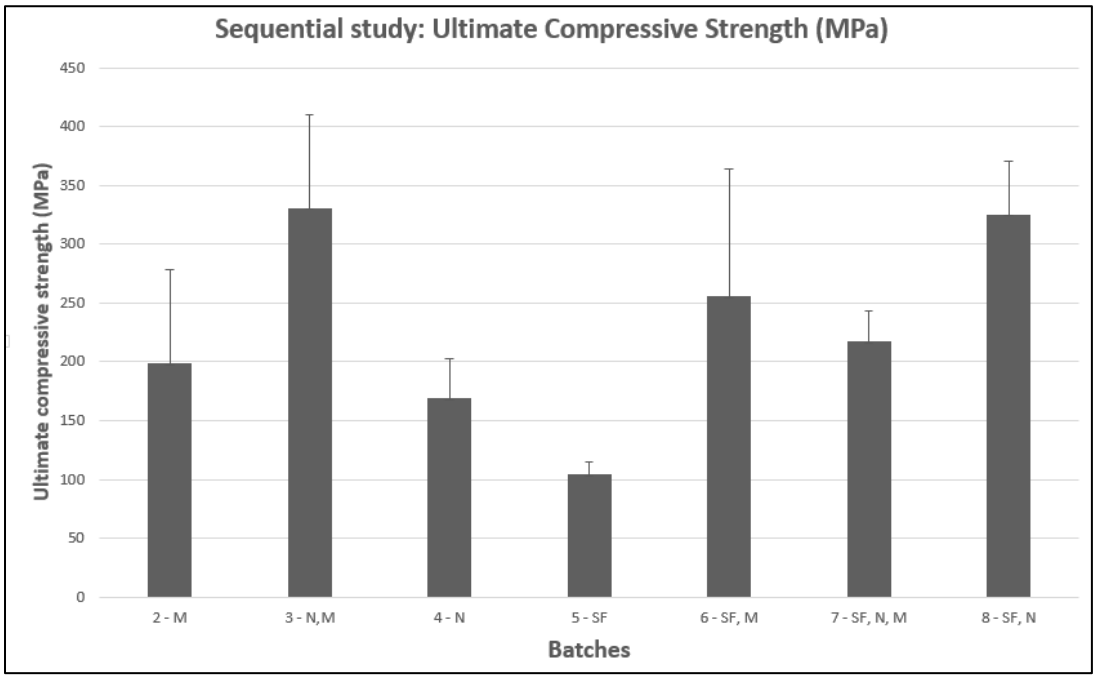

Figure 25: Ultimate compressive strength of different experimental batches.

It can be seen in Figure 26 that the yield strength of Batch 6 is 17.72±7.003 MPa.

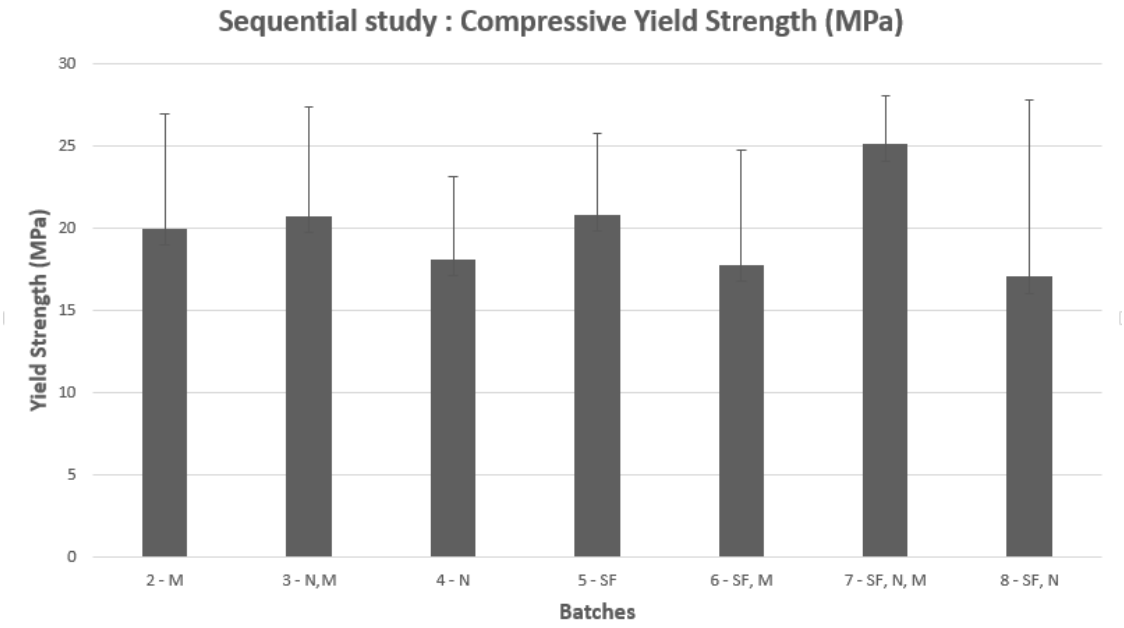

Figure 26: Compressive yield strength of different experimental batches.

The mechanical results for the 9 week degradation study is presented below. No significant difference was observed between the different time points in compression.

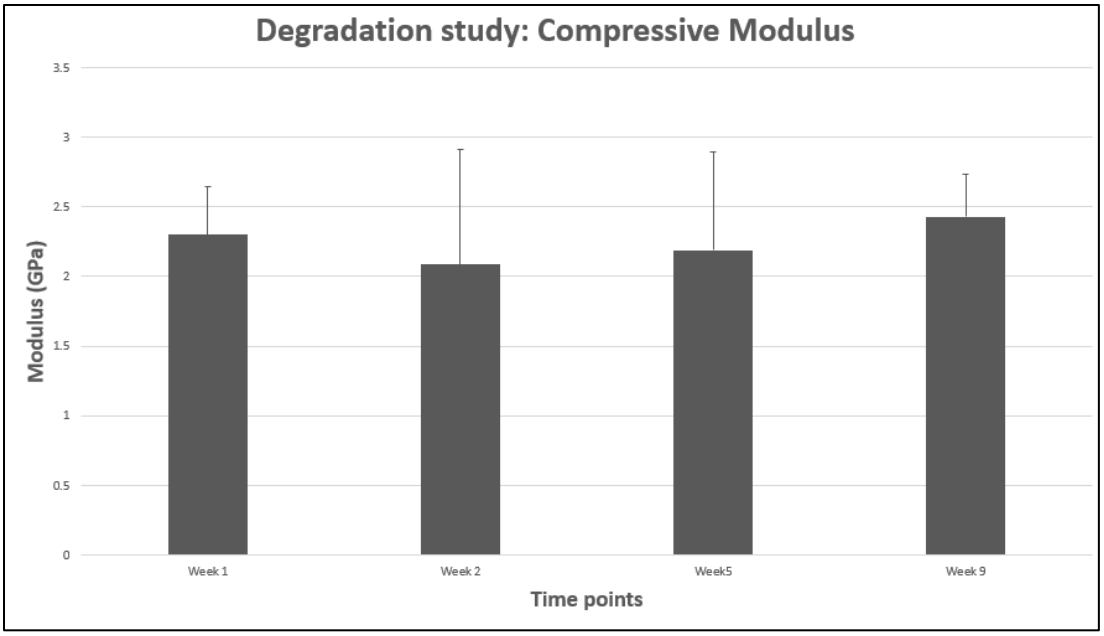

Figure 27: Compressive modulus of scaffolds at different time points.

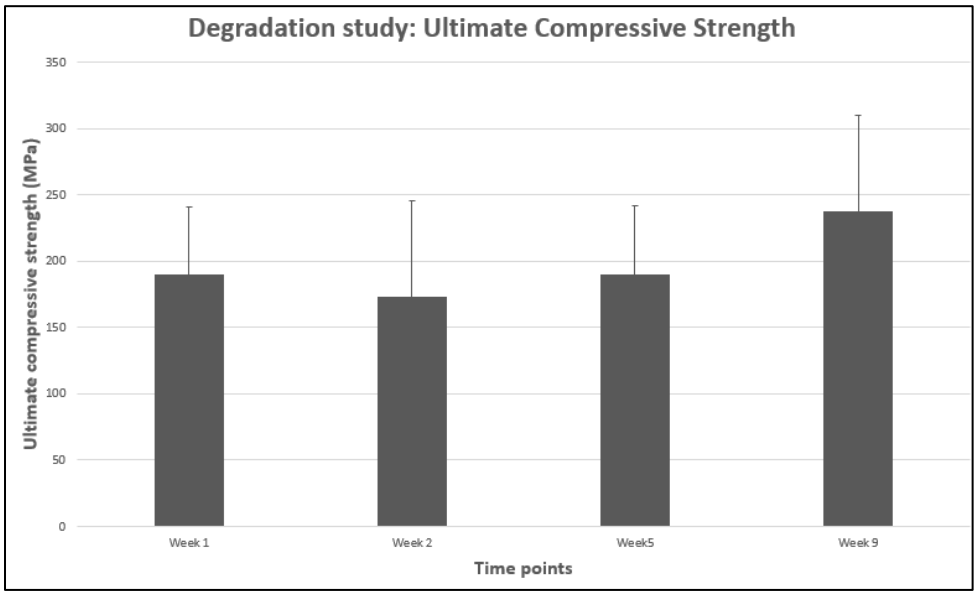

Figure 28: Ultimate Compressive Strength of scaffolds at different time points.

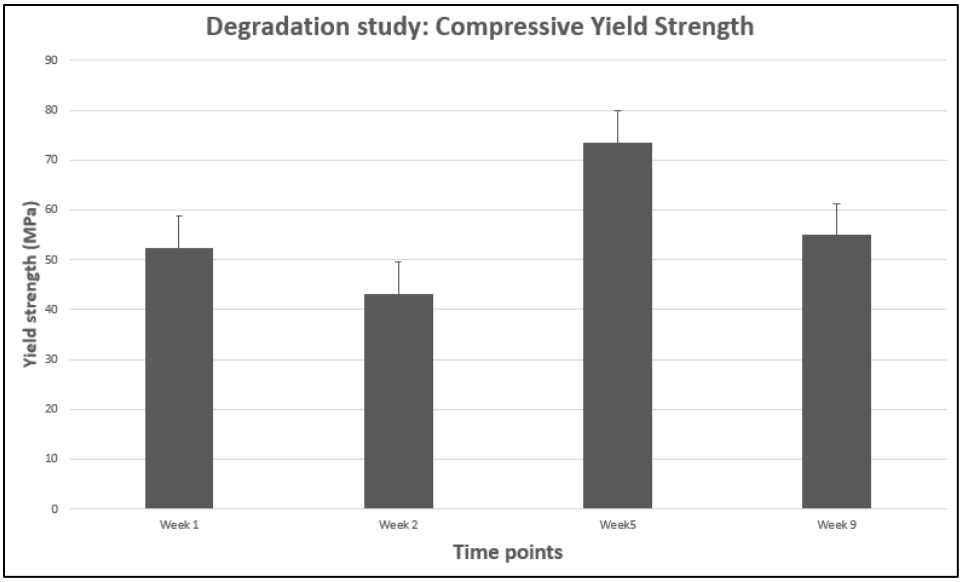

Figure 29: Compressive Yield Strength of scaffolds at different time points.

Whole scaffolds (n=4) were printed and two HAP posts were inserted into opposite ends of two cortical sections as seen in the figure below. The yield strength was seen to be 20.6125±1.91 MPa, the ultimate compressive strength was 20.6125±1.91 MPa, and compressive modulus was 0.2357±0.06121 GPa. The mechanical properties could be low due to soak-freeze that induces pores, as well as the remaining hollow cortical sections. The scaffold which was not soak-frozen or mineralized, and didn't have the two HAP columns was seen to have yield strength of 23.162 MPa, compressive modulus of 0.450 GPa, and compressive strength of 23.162 MPa.

Figure 30: The whole scaffold with two hydroxyapatite posts used for compression testing.

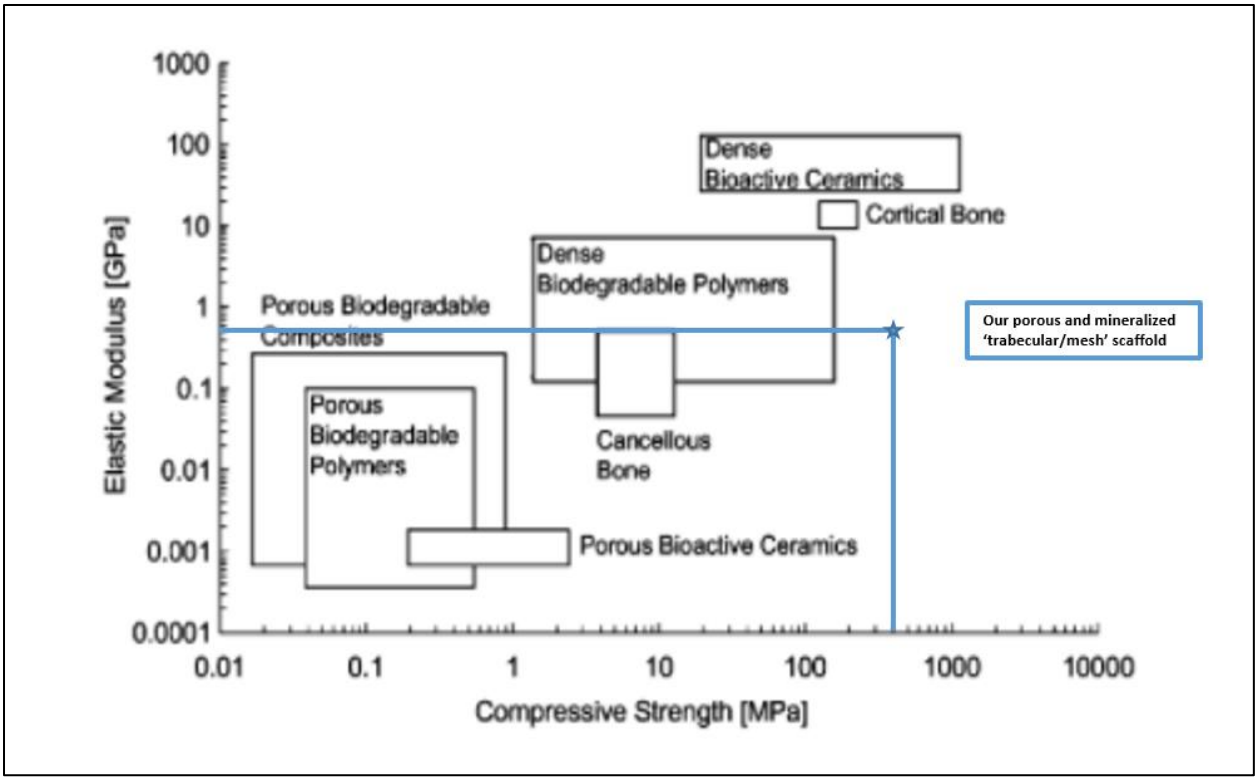

Figure 31: Placement of our 'mesh/trabecular' scaffold's stiffness and mechanical strength in comparison with other material options reviewed in Rezwan et al [43]

2.3.5 Preparing and extruding filaments made of materials other than PLA

Cutting the PLLA after it was cast and allowed to dry was wax-like and would get suck on the insides of the extruder. This was therefore, not usable. The 1:1 ratio of PLA and HAp formed pieces that were then extruded at 140 ˚C. Some of the filaments produced were brittle, and some were too flexible. When printing was attempted, one of the filament was usable in creating the print of half a scaffold before the remaining part filament broke. For the flexible filament it was hard to get the filament into the print head to the nozzle, and the though the heat of the print was modified to the PLA+ HAp temperature of 140 ˚C (from that of PLA at 180-210 ˚C) after a few minutes the filament ceased to flow through the nozzle and curled up within the print head.

2.3.6 Cell Viability

During each cell study presto blue (10x) assay was performed at different time points to check cell metabolism. The total 'n' varied between the different cell studies - but was n=4 per well plate, per group was tested. For each time point scaffold wells, TCP (tissue culture plate with cells) wells, and wells with only presto blue were analyzed. Presto blue assay is minimally toxic and proper washing protocol was ensured pre and post the assay was performed. The time points followed for preliminary HMEC cell study was Day 3, 7, 14 and 21 (Figure 32). The time points followed for final HMEC cell study was Day 4, 8, 11 and 14, (Figure 33) and time points followed for the final HMSC cell study was Day 4, 8 and 12 (Figure 34).

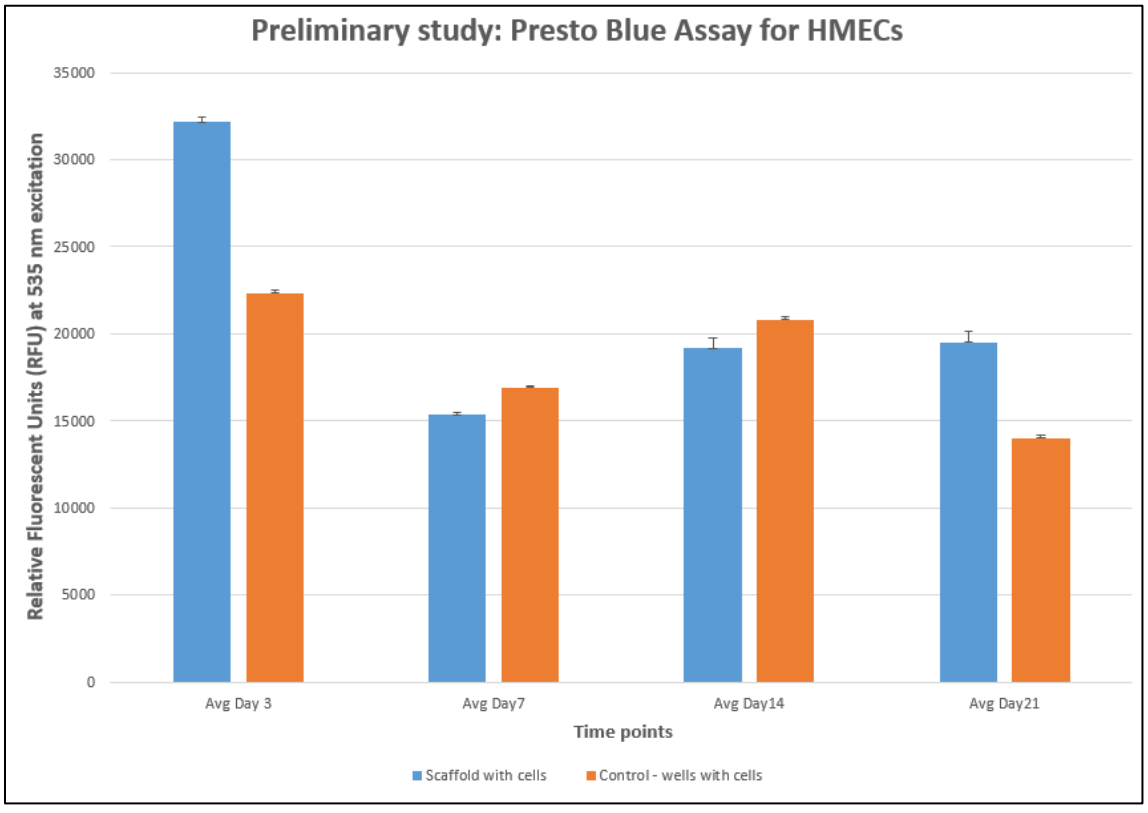

Figure 32: Presto blue assay for preliminary HMEC study with PLA scaffolds and TCP.

HMEC cells on scaffolds are metabolically active through the time of this 21 day study. It is interesting to note that on day 14 both cells on scaffolds as well as TCP begin to be more

metabolically active, and on day 21 the scaffold and cells show more metabolism than the TCP. As mentioned in the methods section, this preliminary study was done as maximum case scenario, therefore the TCP might be less on day 3 due to high confluency, which also might explain the scaffold behavior on days 7 and 12.

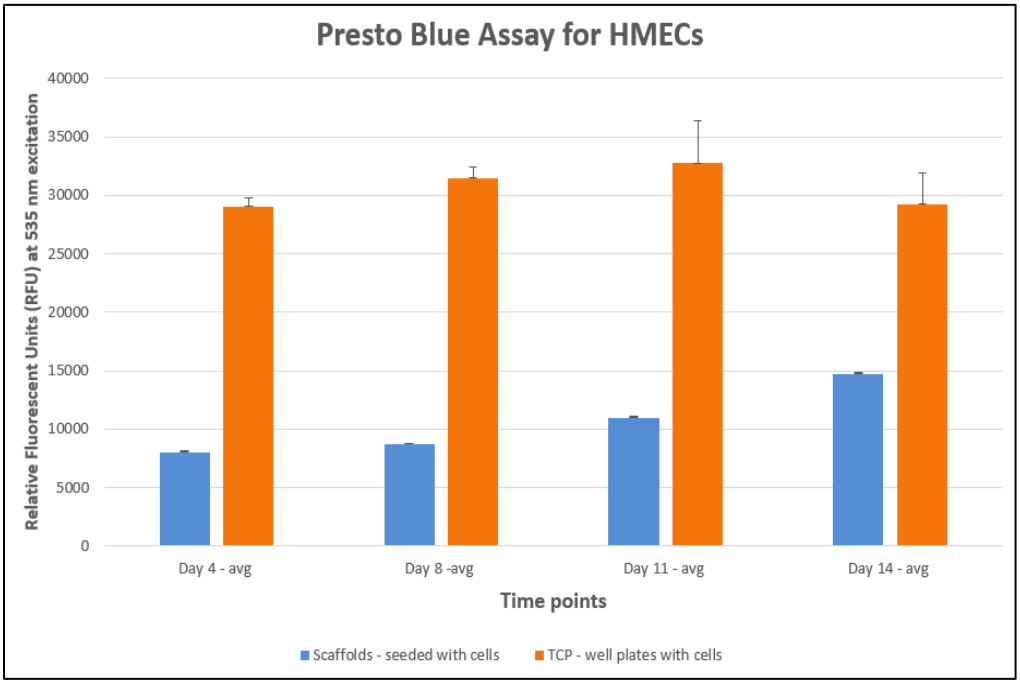

Figure 33: Presto blue assay for final HMEC study PLA scaffolds and TCP.

It can be observed in this final 14 day HMEC study that the cells in the scaffold are definitely increasingly proliferative over the time.

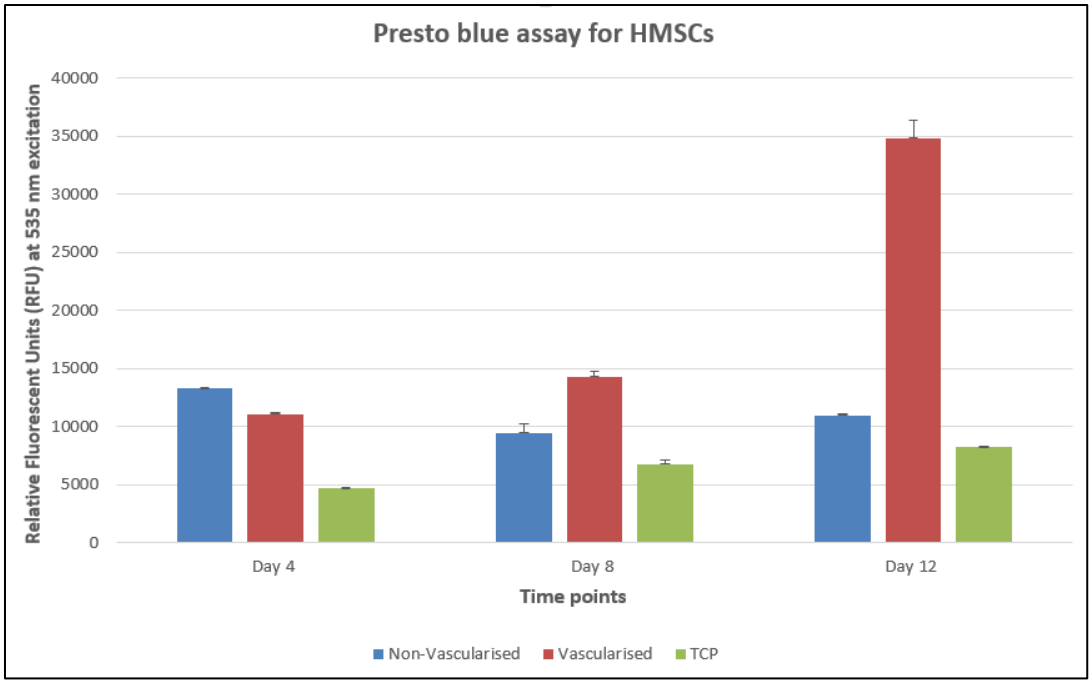

Figure 34: Presto blue assay for final HMSC study PLA scaffolds and TCP.

It can be observed in this final 12 day HMSC study that the cells in the scaffolds are definitely increasingly proliferative over the time. It is interesting to note that both the pre-vascularized and non-vascularized scaffolds performed better than TCP. It also worth noting that the vascular group on Day 12 has extremely high metabolic function.

2.3.7 DAPI and Phalloidin staining

The initial cell study with rat fibroblasts were conducted to assess cell adherence and biocompatibility. DAPI (stains blue) and Phalloidin (stains green) stains were imaged as seen below (Figures 35, 36 and 37) which confirms the presence of cell nuclei and actin fibers.

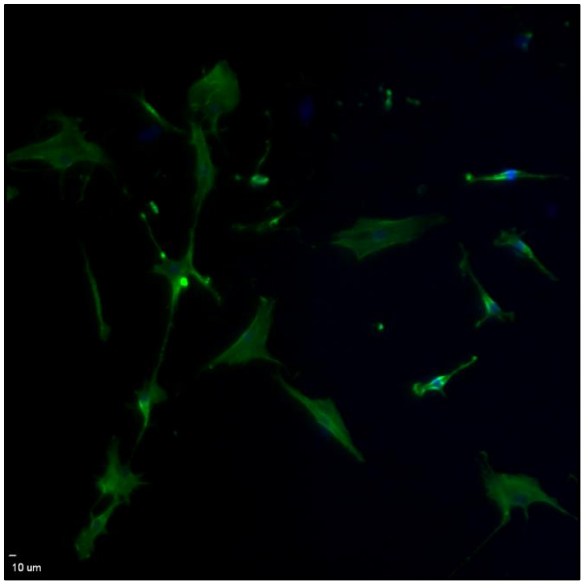

Figure 35: DAPI and Phalloidin image (10x) on TCP, Day 7, seeded and fixed with rat fibroblasts.

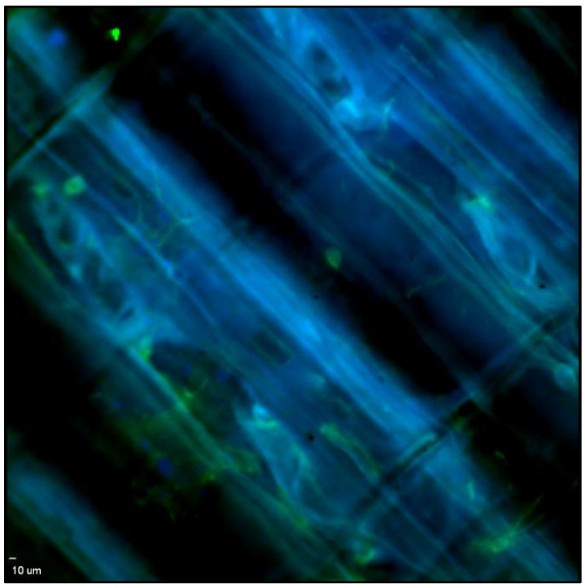

Figure 36: DAPI and Phalloidin image (10x) on scaffold, Day 7, seeded and fixed with rat fibroblasts.

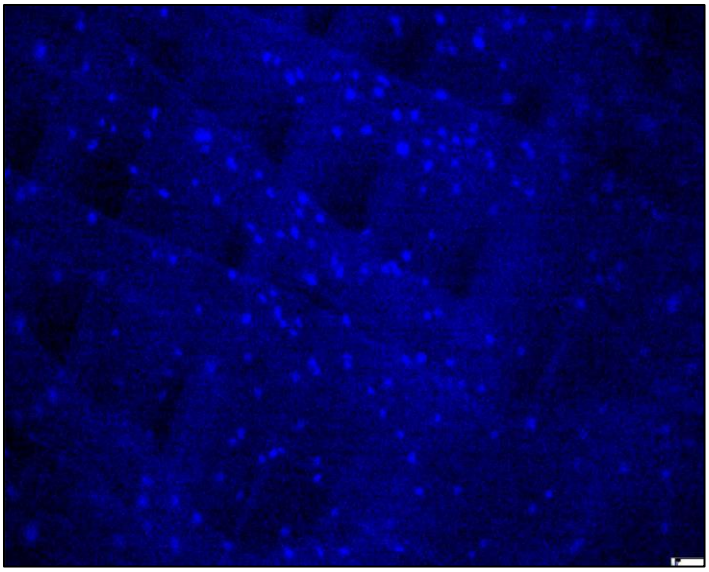

Figure 37: DAPI image (5x) on scaffold, Day 7, seeded and fixed with rat fibroblasts.

2.3.8 Osteocalcin estimation using ELISA

Osteocalcin is a protein crucial to the mineralization of bone, and is characteristic of osteoblasts differentiating to osteocytes. The Osteocalcin kit from Ray Technologies was used for this ELISA.

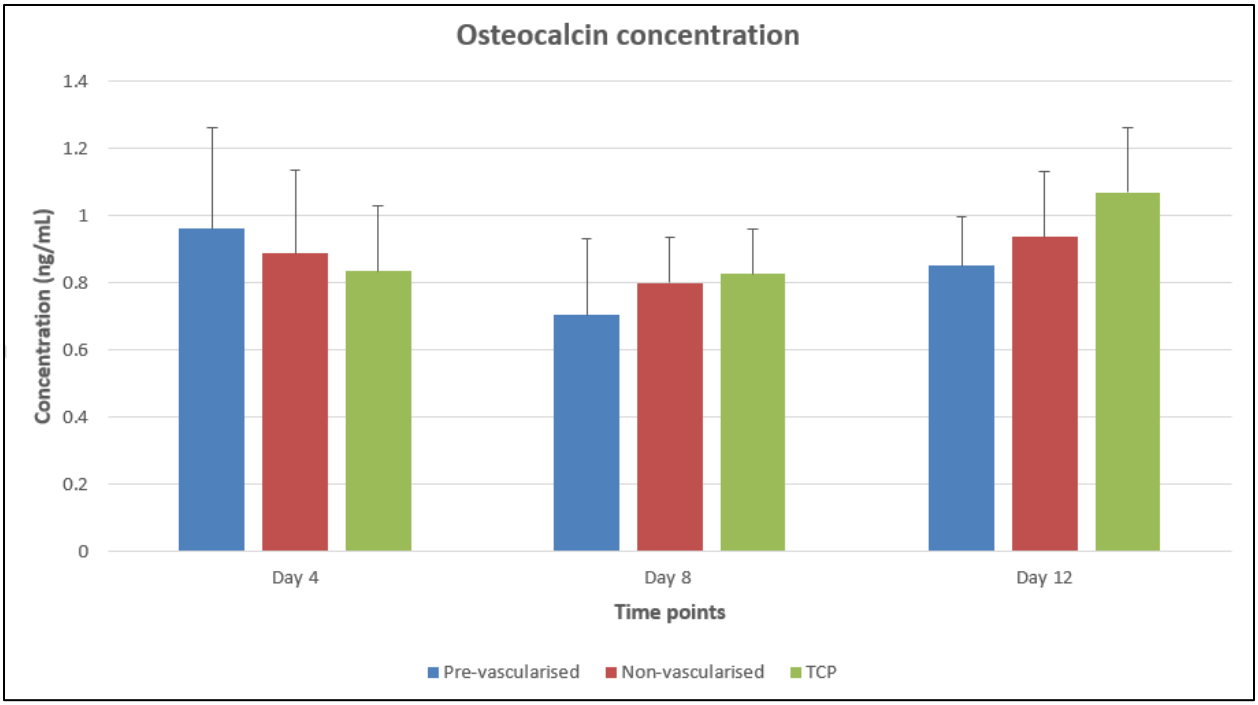

Figure 38: Osteocalcin ELISA result.

Over time non-vascularized scaffolds performed better than vascularized scaffolds in secreting more osteocalcin. It is a late osteogenic marker along with Osteopontin and is believed to start peaking at 21 days. The time points under consideration are Days 4, 8 and 12. This could explain the relatively low concentration of Osteocalcin observed in the Elisa results.

2.3.9 VEGF estimation using ELISA

VEGF or Vascular endothelial growth factor is one of the most prominent angiogenesis stimulatory molecules that induces endothelial cell migration and proliferation. The VEGF kit from Ray Technologies was used for this Elisa.

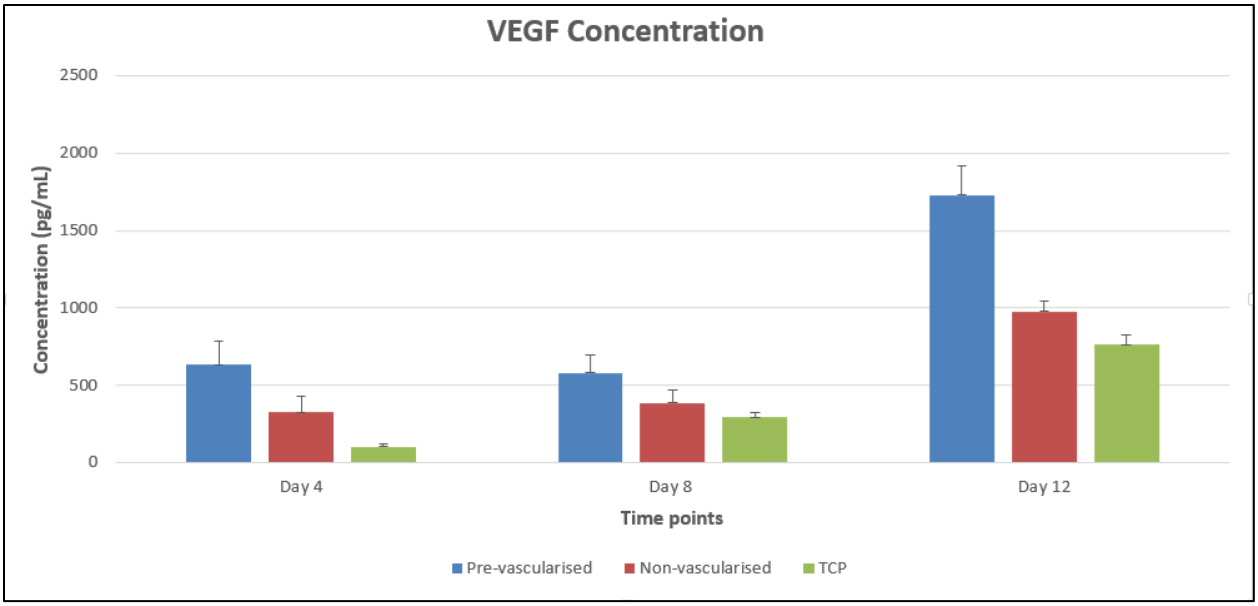

Figure 39: VEGF ELISA result.

It can be observed that pre-vascularized scaffolds out-perform the non-vascularized scaffolds and TCP. This indicates that pre-vascularizing the scaffold enables more MSCs to differentiate into the vascular lineage and produce VEGF.

2.3.10 Alkaline phosphatase (ALP) staining

Alkaline phosphatase (ALP) is a protein expressed during initial cell differentiation phase (Day 5-14). It is an early bone marker that increases initially and then decreases when mineralization is well progressed. [9][10] It was observed that more ALP staining could be spotted easily on non-vascularized scaffolds as opposed to vascularized scaffolds. Day 12 seemed to have more ALP activity that Day 4 and Day 8.

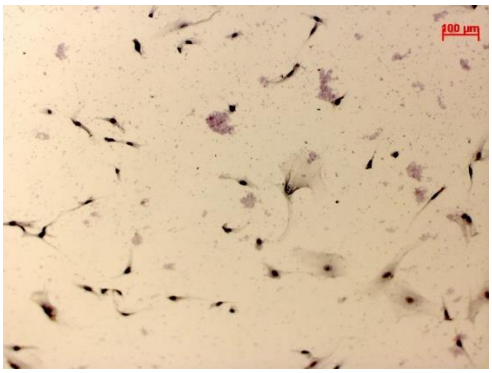

Figure 40: ALP stain image (10x) Day 4, TCP seeded and fixed with HMSCs

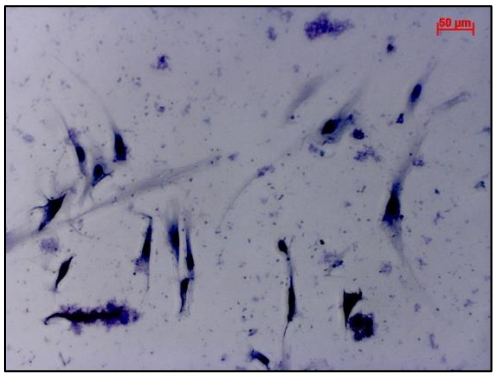

Figure 41: ALP stain image (20x) Day 4, TCP seeded and fixed with HMSCs

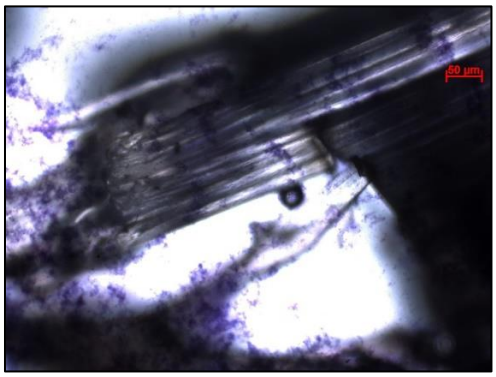

Figure 42: ALP stain image (20x) Day 4, non-vascularized scaffold seeded and fixed with HMSCs (cut scaffold)

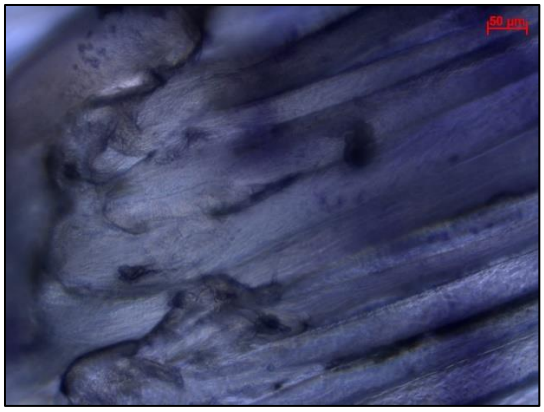

Figure 43: ALP stain image (40x) Day 4, non-vascularized scaffold seeded and fixed with HMSCs (cut scaffold)

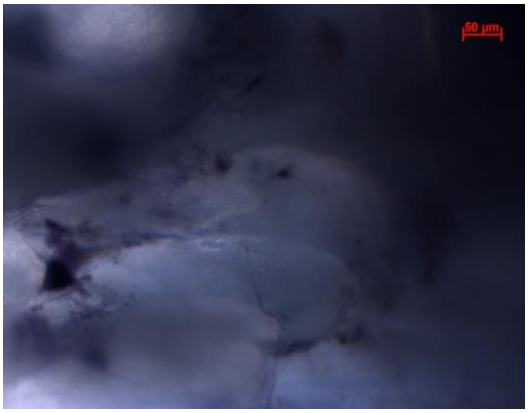

Figure 44: ALP stain image (40x) Day 4, vascularized scaffold seeded and fixed with HMSCs (cut scaffold)

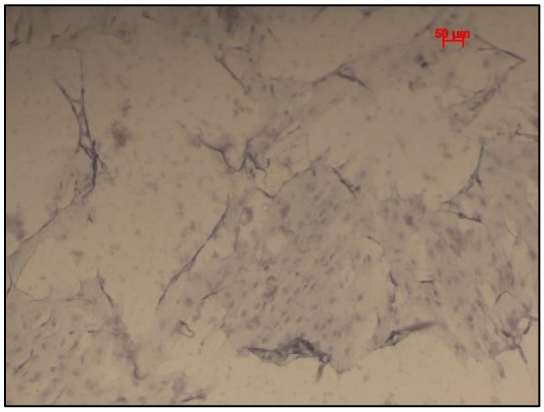

Figure 45: ALP stain image (10x) Day 8, TCP seeded and fixed with HMSCs

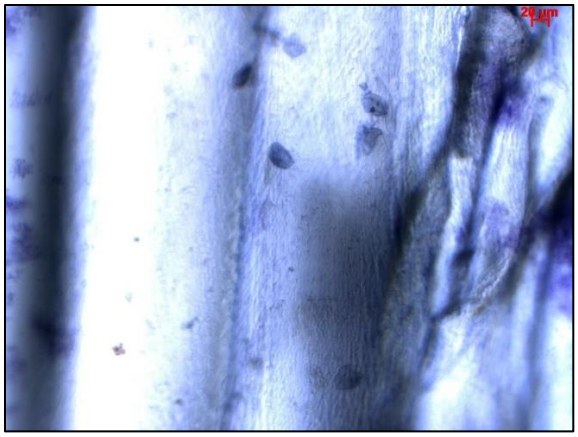

Figure 46: ALP stain image (20x) Day 8, non-vascularized scaffold seeded and fixed with HMSCs (cut scaffold)

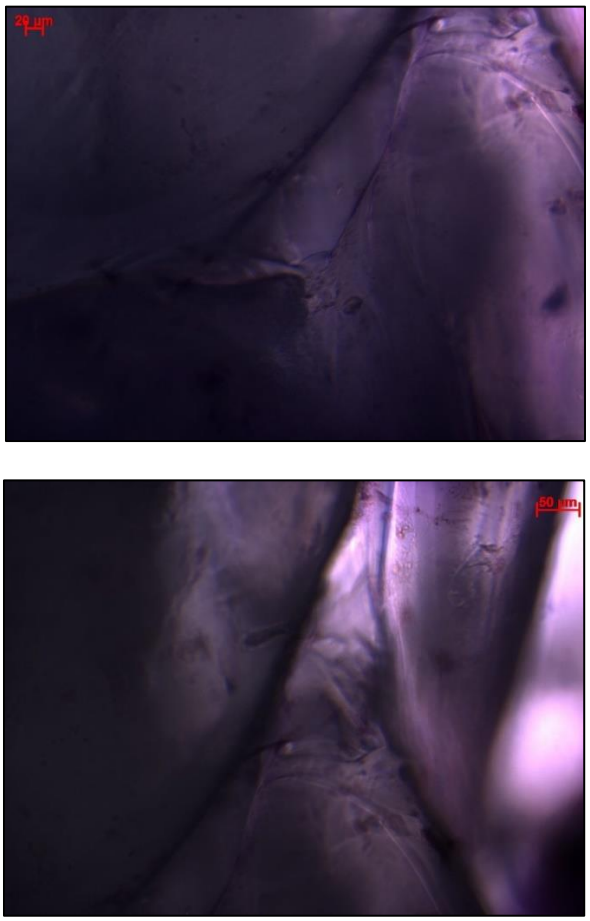

Figure 47: ALP stain image (20x) Day 8, vascularized scaffold seeded and fixed with HMSCs (cut scaffold)

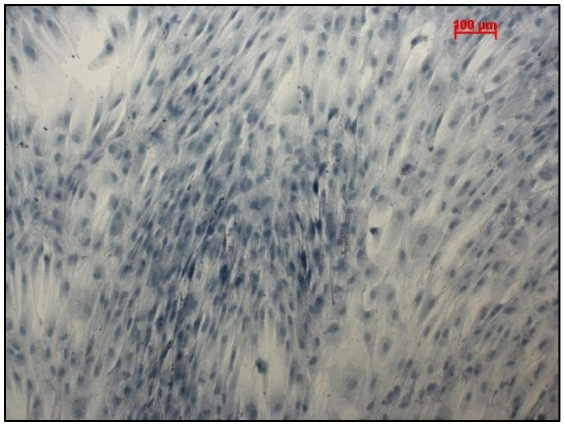

Figure 48: ALP stain image (10x) Day 12, TCP seeded and fixed with HMSCs

Figure 49: ALP stain image (40x) Day 12, non-vascularized scaffold seeded and fixed with HMSCs (uncut scaffold)

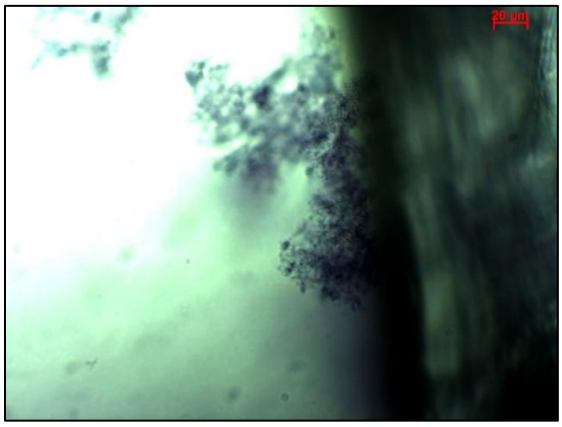

Figure 50: ALP stain image (40x) Day 12, vascularized scaffold seeded and fixed with HMSCs (uncut scaffold)

2.3.11 CD31

CD31 is an integral membrane protein that is expressed on the surface of endothelial cells. It mediates cell-cell adhesion and interactions involving angiogenesis. Scaffolds from Day 14 of HMEC cell study were observed for CD31 and the presence can be seen in the pictures below. It is clearly seen on the TCP image below, along with DAPI. Scaffolds from Days 4, 8, and 12 from the HMSC study were also stained and can be observed below. DAPI stains blue, and CD31 stains pink. The presence of CD31 is higher in pre-vascularised scaffolds when compared with non-vascularized scaffolds. Day 8 and Day 12 show more presence of CD31 as opposed to Day 4.

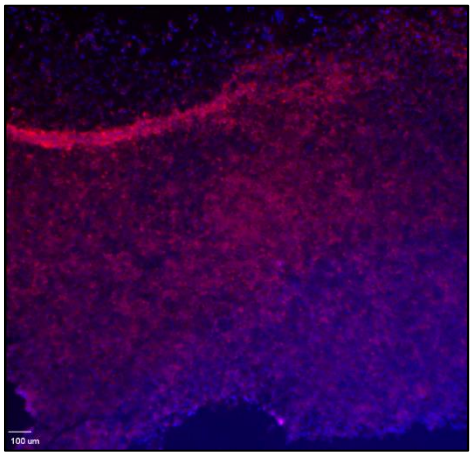

Figure 51: CD31 and DAPI fluorescent image (4x) on Day 14 seeded and fixed with TCP.

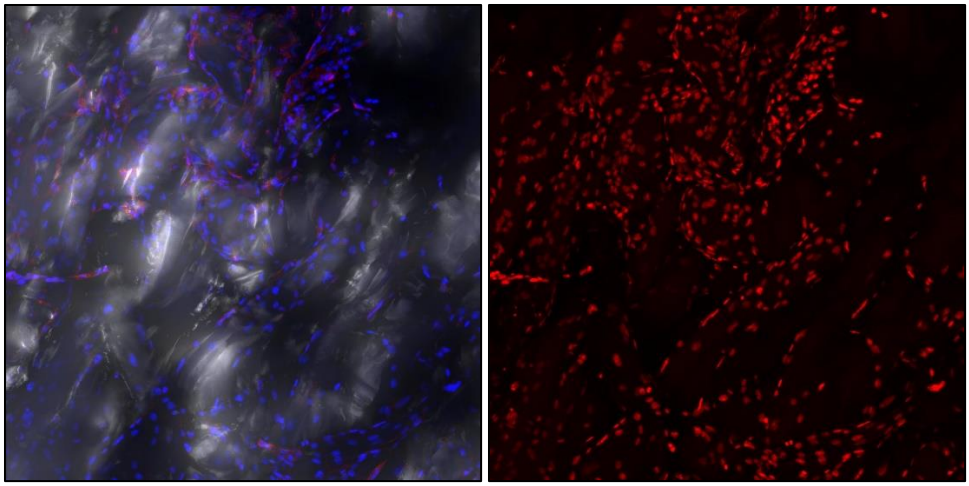

Figure 52: CD31 and DAPI fluorescent image (10x) of scaffold seeded and fixed with HMECs (Day 14). Left: CD31 (pink), DAPI blue. Right: Only CD31 (red).

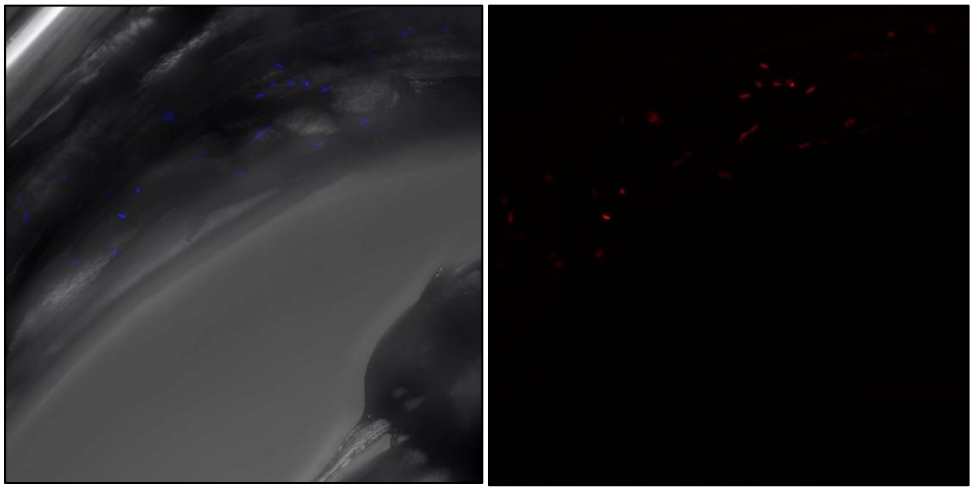

Figure 53: CD31 and DAPI fluorescent image (10x) of non-vascularized scaffold seeded and fixed with HMSCs (Day 4). Left: CD31 (pink), DAPI blue. Right: Only CD31 (red).

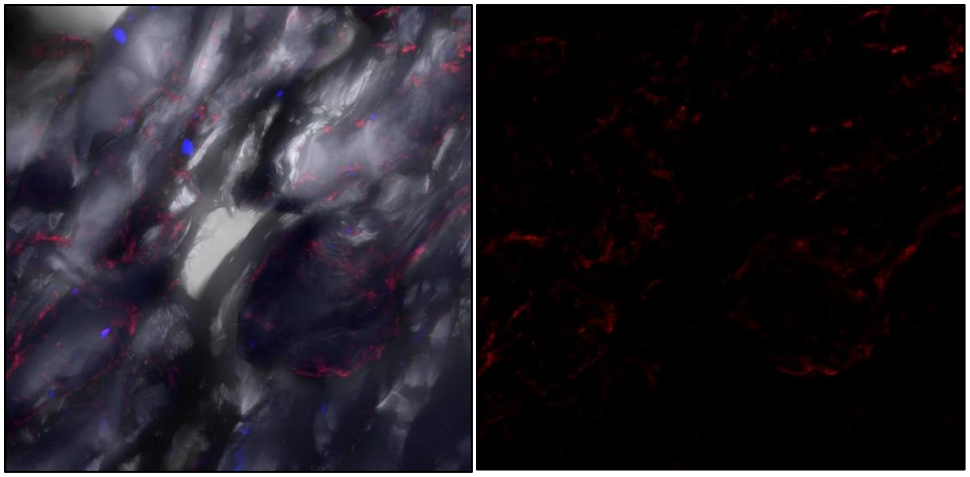

Figure 54: CD31 and DAPI fluorescent image (10x) of vascularized scaffold seeded and fixed with HMSCs (Day 4). Left: CD31 (pink), DAPI blue. Right: Only CD31 (red).

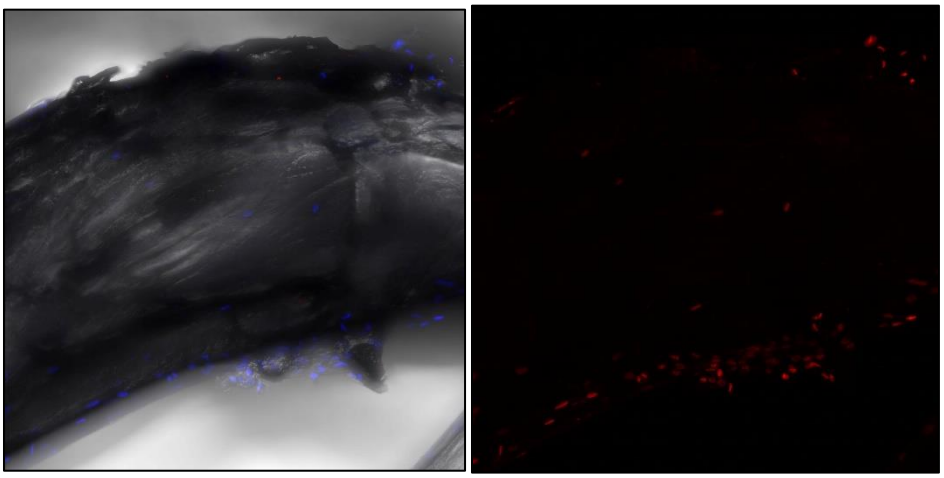

Figure 55: CD31 and DAPI fluorescent image (10x) of non-vascularized scaffold seeded and fixed with HMSCs (Day 8). Left: CD31 (pink), DAPI blue. Right: Only CD31 (red).

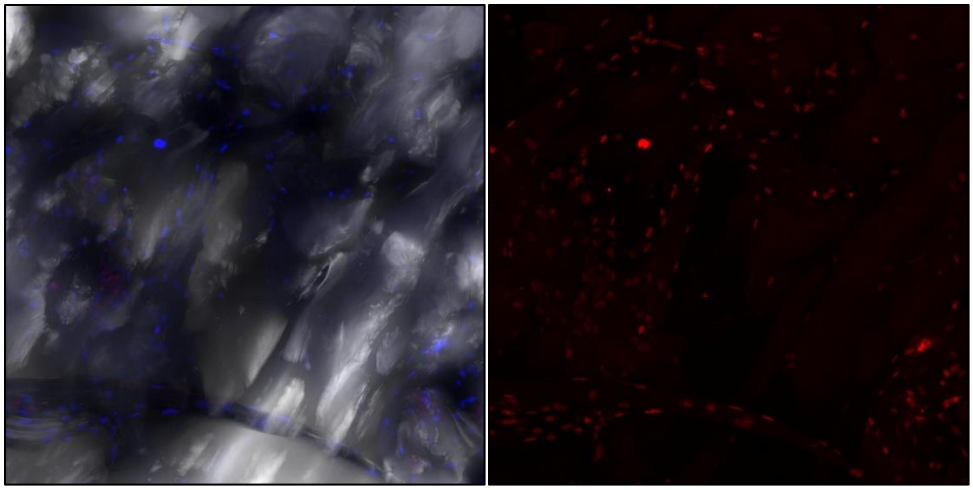

Figure 56: CD31 and DAPI fluorescent image (10x) of vascularized scaffold seeded and fixed with HMSCs (Day 8). Left: CD31 (pink), DAPI blue. Right: Only CD31 (red).

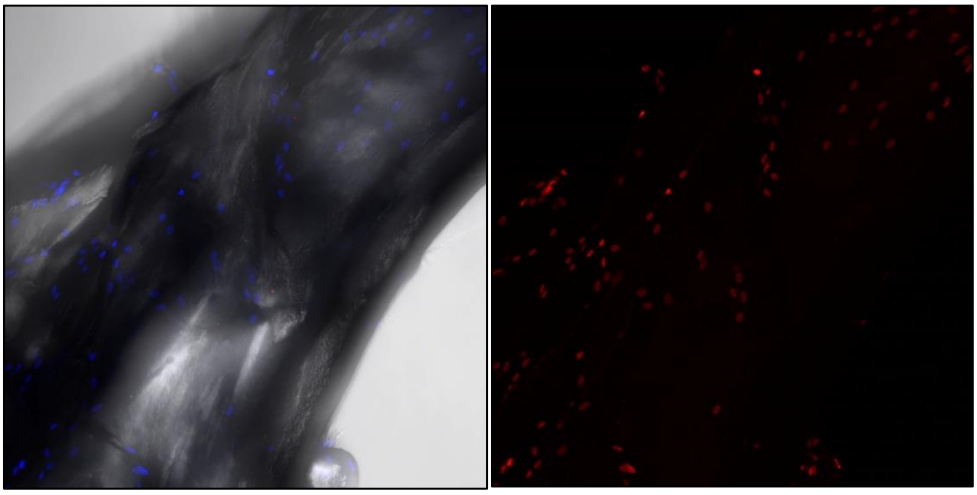

Figure 57: CD31 and DAPI fluorescent image (10x) of non-vascularized scaffold seeded and fixed with HMSCs (Day 12). Left: CD31 (pink), DAPI blue. Right: Only CD31 (red).

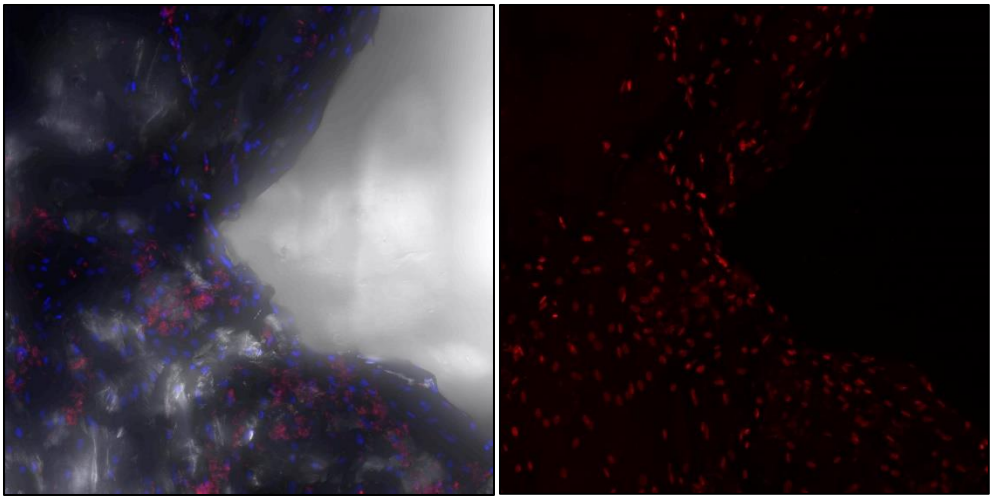

Figure 58: CD31 and DAPI fluorescent image (10x) of vascularized scaffold seeded and fixed with HMSCs (Day 12). Left: CD31 (pink), DAPI blue. Right: Only CD31 (red).

2.3.12 Discussion

Groups [8] [17] have reported 3D printed designs similar to the central 'mesh'/'trabecular' the bone scaffold (with circular instead of rectangular struts), but to our knowledge no group has reported a 3D printed scaffold having a cortical and whole bone scaffold design such as ours. With respect to printing, it is advisable to print the first layer at a safe speed less than or equal to 30%, and adjust the fan speed and build plate temperature as required, and monitor the progress. For the first print of a new design, it is recommended to monitor the print progress even after the first layer as it helps avert possible problems. If this is not done, the print might fail and a lot of material gets wasted depending on the size of the print. An additional consideration would be that for printing bone scaffolds with emphasis on small dimensional pores size, shape and quality, it is better to design in bigger dimensions and then scale down during slicing, rather than designing in smaller required dimensions. Once the design print is executed perfectly, it is easy to print multiple copies sequentially or together without continuous monitoring, depending upon the complexity of the design. It is observed that for each type of filament (clear/natural/transparent), the printing properties might have to be altered to get the required print quality.

The gap between the rectangular struts in the trabecular/mesh/central portion of the scaffold is 300-350 µm which is optimal for osteoblast growth.

The soak-freeze technique is a simple and effective idea where scaffolds are soaked before being placed in a freezer. The scaffolds are thus first placed in -20 ˚C which induces formation of macro pores, and then are placed in the -80 ˚C freezer which induces formation of micro pores. Of special interest are the 5 µm pores formed while in the -80 ˚C freezer that will support vascularization, further tissue development throughout the scaffold and increased space for mineralization throughout the scaffold.

The sequential pre-treatment method selected was that of soak-freeze and mineralize. No group has reported soaking and freezing in two different temperatures sequentially to achieve pore formation.

Another group has used liquid nitrogen and a -40 ˚C freezer for creation of pores, however, they do not soak the scaffold prior to freezing; in order to enhance pore creation from the growth of more ice crystals we soaked our scaffolds in water prior to freezing. [75]

The compression testing from the sequential treatments with trabecular/mesh scaffold revealed that the mechanical strength is good - the stiffness and mechanical strength is more than that of human trabecular bone, and that of whole scaffold is comparable to the cancellous bone. Another point of note is the fact that there is no difference between mechanical properties of the soak-freeze scaffold reinforced with two hydroxyapatite posts and the scaffold without the soak-freeze and posts. What this implies is that the decrease in mechanical properties induced by pore formation in soak-freeze is compensated for by the addition of the two posts. Adding more HAP posts, and designing some of the cortical sections to be solid instead of hollow should improve the mechanical properties even more.

The degradation study shows that for the first five weeks there is no significant decrease in mineralization, which implies that there is no compromise in bone growth support for more than a

month. The mechanical properties do not decrease significantly up to nine weeks, which implies that the mechanical integrity of the construct is the same for more than 2 months.

Stem cells are undifferentiated cells with a high proliferation capability; they are capable of self-renewal, and multi-lineage differentiation regeneration of tissues. [63] They have varying degrees of differentiation potential. MSCs respond to micro environmental changes and adjust their pathway accordingly. Once cues from vascular cells have been introduced (through the production of vascular tissue before decellularization, MSCs have the ability to integrate into the forming vessels in the surrounding bone by differentiating along endothelial cell lineage. [67] This is observed in the VEGF ELISA results which show that the pre-vascularized scaffolds ensure MSCs to differentiate along the endothelial lineage.

Thus, a biomimetic environment is created. This VEGF data is complemented by the presto blue data in the HMSC cell study which shows increased cell metabolism to exist in seeded scaffolds. This is also seen by the data presented in the osteocalcin ELISA.

ALP staining and CD31 imaging show a positive presence thus reinforcing the presence of vascular and bone cells respectively. Osteoinductive properties are observed by the HMSCs differentiating into bone forming osteoblasts leading to osteogenesis. The scaffold design thus has good osteoconduction and osteoinductive cues to attract the patient's own stem cells after implantation thereby eliminating the need for exogenous GFs and cell delivery. Load bearing capabilities are shown by compression data. Vascularity is thus shown by presto blue, VEGF and CD 31 data. Osteoconductive and osteoinductive properties are confirmed by presto blue, Osteocalcin and ALP data.

CHAPTER 3 – Conclusions and Future Direction

Conclusions

This project lead to the design and development of a pre-vascularized, load bearing, highly porous three dimensional scaffold made of biodegradable and biocompatible material, promoting vascular ingrowth, osteoblast adhesion, growth and differentiation, and bone tissue formation.

The scaffold design thus has good osteoconduction and osteoinductive cues to attract the patient's own stem cells after implantation thereby eliminating the need for exogenous GFs and cell delivery.

It addresses the issues faced by the current options such as autografts and allografts, as well as most synthetic grafts.

Thus the bone scaffolds developed in this project is among the cutting edge bone grafting options available today can be used to treat bone defects and restore function of traumatized and damaged bone.

Future Direction

From the CD31 data it can be understood that a higher seeding density (preferably around 50,000 cells per cm square) would be more preferable.

Flow mineralization should be carried out on the scaffolds to assess the difference and advantages over static mineralization followed in this project.

Bone scaffolds have to be in low oxygen tension in vivo as there is a lack of adequate vasculature (0-3% oxygenation). In vitro testing conditions should be modified to accommodate this oxygen tension level to get better corroboration with possible in-vivo results. [76]

Minor design changes to the final scaffold wherein some of the cortical portions are printed as solid instead of hollow to improve mechanical properties.

PLA has been shown to undergo bulk erosion which is not good for an implant – and therefore this has to be investigated for the exact scaffold design.

It is reported that MSCs co-cultured with osteocytes leads to higher calcium deposits and ALP expression, and faster differentiation into bone cells. [9] This could be considered for animal studies in the future while implanting this 3D printed bone scaffold.

Cbfa1, an early osteogenic differentiation marker could be tested – this coupled with the VEGF Elisa could help assess the path taken by the MSCs more clearly early on in the cell study –i.e. if the seeded scaffolds support a vascularization pathway more than a osteogenic pathway.

PLA can be mixed with HAp in different ratios – a 1:1 ratio was made, casted and extruded. Extrusion worked for two of the batches, but printing was hard due to filaments snapping or curling up. Curing the filaments by immersing in hot water at 120 ˚C helped make it less brittle. A lower concentration of HAp could be casted with PLA and extruded as a filament, and then used to print the design. It is an iterative process to see assess the optimal ratio suitable for printing.

REFERENCES

1. Ning ZHU, David COOPER , Xiong-Biao CHEN, and Catherine Hui NIU, A study on the in vitro degradation of poly(L-lactide)/chitosan microspheres scaffolds. (Degradation study)
2. Raviraj Havaldar, S.C. Pilli and B.B.Putti, Insights into the effects of tensile and compressive loadings on human femur bone. (half-baked explanation written somewhere in the thesis)
3. Antonio J.Salgado, Olga P.Coutinho, Rui L.Reis, 'Bone Tissue Engineering: State of the Art and Future Trends'. (Scroot ref 1)
4. M. J. Yaszemski, J. B. Oldham, L. Lu, B. L. Currier, ''Bone Engineering'', 1st edition, Em squared, Toronto 1994, p. 541. (Scroot ref 1's ref 30).
5. Eva Johanna Kubosch, Anke Bernstein, Laura Wolf, Tobias Fretwurst, Katja Nelson, and Hagen Schmal, 'Clinical trial and in-vitro study comparing the efficacy of treating bony lesions with allografts versus synthetic or highly-processed xenogeneic bone grafts'.
6. Mistry AS, Mikos AG. Tissue engineering stratergies for bone regeneration, Adv Biochem Biotechnol 2005;94:1-22.
7. Christopher G. Finkemeier, Bone-Grafting and Bone-Graft Substitutes, Current Concepts Review.
8. Andrew C. Daly , Gráinne M. Cunniffe , Binulal N. Sathy , Oju Jeon , Eben Alsberg , and Daniel J. Kelly. 3D Bioprinting of Developmentally Inspired Templates for Whole Bone Organ Engineering.
9. E. Birmingham1,2, G.L. Niebur2,3, P.E. McHugh1,2, G. Shaw2,3, F.P. Barry 2,3 and L.M. McNamara1,2*. Osteogenic Differentiation Of Mesenchymal Stem Cell Is Regulated By Osteocyte and Osteoblast Cells In A Simplified Bone Niche.
10. Jane E. Aubin., 'Regulation Of Osteoblast Formation and Function'.
11. Yu-Tzu Tsao 1,2, Yi-Jeng Huang 3, Hao-Hsiang Wu 3, Yu-An Liu 4, Yi-Shiuan Liu 4,*and Oscar K. Lee 1,4,5,6,7,*, Osteocalcin Mediates Biomineralization during Osteogenic Maturation in Human Mesenchymal Stromal Cells.
12. *Dr. Kamran Zamanian, Brett McKitterick, and Dylan Freeze, iData Research Inc,* 'Orthopedic Biomaterial Bone Graft Market To Increase With Stem Cell Therapy Market Growth'. (Report)
13. Schwebel, Goetz, and Sieben, Broken Bone Injuries. (Report)
14. Seou Lee1† , Taehoon Kwon2† , Eun Kyung Chung2 and Joon Woo Lee2*, 'The market trend analysis and prospects of scaffolds for stem cells'.
15. PR Newswire, PR Newswire US, 08/17/2017
16. Nelson Laboratories, 'Sterilization and Biocompatibility of 3D-Printed Orthopedic Devices: Testing Considerations.
17. Ethan Nyberg, BS, Alexandra Rindone, BS, Amir Dorafshar, MBchB, Warren L. Grayson, PhD, 'Comparison of 3D-Printed Poly-ε-Caprolactone Scaffolds Functionalized with Tricalcium Phosphate, Hydroxyapetite, Bio-Oss, or Decellularised Bone Matrix.
18. Temple JP[1], Hutton DL, Hung BP, Huri PY, Cook CA, Kondragunta R, Jia X, Grayson WL., Engineering anatomically shaped vascularized bone grafts with hASCs and 3D-printed PCL scaffolds.
19. Taylor BL, Limaye A, Yarborough J, Freeman JW. 2016. Investigating processing techniques for bovine gelatin electrospun scaffolds for bone tissue regeneration. J Biomed Mater Res Part B 2016:00B: 000-000.
20. Tas AC, Bhaduri SB, Rapid coating of Ti6A14V at room temperature with a calcium phosphate solution similar to 10x simulated body fluid. J Mater Res 2004;19-2742 -2749.

21. Tea Andric, Lee D. Wright, Joseph W. Freeman, 'Rapid Mineralisation of Electrospun Scaffolds for Bone Tissue Engineering.
22. T. Patrıcio and M. Domingos, A. Gloria and U. D'Amora, J.F. Coelho, P. J. B artolo., Fabrication and characterisation of PCL and PCL/PLA scaffolds for tissue engineering.
23. Meseguer-Olmo L, Vicente-Ortega V, Alcaraz-Baños M, Calvo-Guirado JL, Vallet-Regí M, Arcos D, Baeza A. 2013. *In-vivo* behavior of Si-hydroxyapatite/polycaprolactone/DMB scaffolds fabricated by 3D printing. J Biomed Mater Res Part A 2013:101A:2038–2048
24. Timothy M. Rankin, MD,[1] Nicholas A. Giovinco, DPM,[2] Daniel J. Cucher, MD,[1] George Watts, PhD,[3] Bonnie Hurwitz, PhD,[1,4] and David G. Armstrong, MD, PhD, DPM[2,] 3D printing surgical instruments: Are we there yet?
25. Athanasiou KA[1], Niederauer GG, Agrawal CM., Sterilization, toxicity, biocompatibility and clinical applications of polylactic acid/polyglycolic acid copolymers.
26. Rozema FR[1], Bos RR, Boering G, van Asten JA, Nijenhuis AJ, Pennings AJ., The effects of different steam-sterilization programs on material properties of poly(L-lactide).
27. Nair L.S., Laurencin C.T. (2005) Polymers as Biomaterials for Tissue Engineering and Controlled Drug Delivery. In: Lee K., Kaplan D. (eds) Tissue Engineering I. Advances in Biochemical Engineering/Biotechnology, vol 102. Springer, Berlin, Heidelberg. (write up from pla doc, I think)
28. M. Savioli Lopesa,b a*, A. L. Jardinib , R. Maciel Filhoa,b., Poly (lactic acid) production for tissue engineering applications. (write up from pla doc)
29. LIU Yunfeng, ZHU Fudong, ZHU Huiyong,. Review on Techniques of Design and Manufacturing for Bone Tissue Engineering Scaffold.
30. Langer R, Vacanti JP. Tissue engineering. Science,1993, 260(5110) : 920–92.
31. Wang HV, Johnston SR, Rosen DW, et al. Design of a graded cellular structure for an acetabular hip replacement component. In: Solid Freemform Fabrication Proceedings, 111-123, 2006, Austin, USA
32. Molly M. Stevens,. Biomaterials for bone tissue engineering.
33. Dalby, M. J., et al., Nat. Mater. (2007) 6, 997
34. Levenberg, S., et al., Nat. Biotechnol. (2005) 23, 879
35. Feyza Engin and Brendan Lee,. NOTCHing the bone: Insights into multi-functionality
36. Zanetti AS, Sabliov C, Gimble JM, Hayes DJ 2013. Human adipose-derived stem cells and three dimensional scaffold constructs: A review of the biomaterials and models currently used for bone regeneration. J Biomed Mater Res Part B 2013:101B:187–199.
37. Lendeckel S, Jodicke A, Christophis P, Heidinger K, Wolff J, Fraser JK, Hedrick MH, Berthold L, Howaldt HP. Autologous stem cells (adipose) and fibrin glue used to treat widespread traumatic calvarial defects: Case report. J Craniomaxillofac Surg 2004;32:370–373.
38. Taylor JA. Bilateral orbitozygomatic reconstruction with tissue engineered bone. J Craniofac Surg 2010;21:1612–1614.
39. Mesimaki K, Lindroos B, Tornwall J, Mauno J, Lindqvist C, Kontio R, Miettinen S, Suuronen R. Novel maxillary reconstruction with ectopic bone formation by GMP adipose stem cells. Int J Oral Maxillofac Surg 2009;38:201–209.
40. Thesleff T, Lehtimaki K, Niskakangas T, Mannerstrom B, MiettinenS, Suuronen R, Ohman J. Cranioplasty with adipose-derived stem cells and biomaterial: A novel method for cranial reconstruction. Neurosurgery 2011;68:1535–1540.
41. Reichert JC, Hutmacher DW. Bone tissue engineering. In: Pallua, editor. Tissue Engineering; Springer, 2011. p 643.
42. Gaalen S, Kruyt M, Meijer G, Mistry A, Mikos A, Beucken J, Jansen J, Groot K, Cancedda R, Olivo C, Yaszemski M, Dhert W. Tissue engineering of bone. In: Clemens van Blitterswijk, editor. Tissue Engineering; Academic Press, 2008. p 740.

43. K. Rezwana, Q.Z. Chena, J.J. Blakera, Aldo Roberto Boccaccinia,b,. Biodegradable and bioactive porous polymer/inorganic composite scaffolds for bone tissue engineering.
44. Bergsma EJ, Rozema FR, Bos RRM, Debruijn WC. Foreign body reaction to resorbable poly(L-lactic) bone plates and screws used for the fixation of unstable zygomatic fractures. J Oral Maxillofac Surg 1993;51:666–70
45. Martin C, Winet H, Bao JY. Acidity near eroding polylactidepolyglycolide in vitro and in vivo in rabbit tibial bone chambers. Biomaterials 1996;17(24):2373–80.
46. Jagur-Grodzinski J. Biomedical application of functional polymers.Reactive Funct Polym 1999;39:99–138.
47. Rich J, Jaakkola T, Tirri T, Narhi T, Yli-Urpo A, Seppala J. In vitro evaluation of poly([var epsilon]-caprolactone-co-DL-lactide)/bioactive glass composites. Biomaterials 2002;23:2143–50.
48. de Groot K, Lein CPAT, Wolke JGC, de Bliek-Hogervost JMA. Chemistry of calcium phosphate bioceramics. In: Yamamuro T, Hench LL, Wilson J, editors. Handbook of bioactive ceramics. Boca Raton, FL: CRC Press; 1990. p. 3–16.
49. R. Langer and D. A. Tirrell, “Designing materials for biology and medicine,” Nature, vol. 428, no. 6982, pp. 487–492, 2004.
50. J. R. Fuchs, B. A. Nasseri, and J. P. Vacanti, “Tissue engineering: a 21st century solution to surgical reconstruction,”
51. Annals of Thoracic Surgery, vol. 72, no. 2, pp. 577–591, 2001. B. D. Boyan, T. W. Hummert, D. D. Dean, and Z. Schwartz, “Role of material surfaces in regulating bone and cartilage cell response,” Biomaterials, vol. 17, no. 2, pp. 137–146, 1996.
52. C. A. L´eon y Le ´ on, “New perspectives in mercury porosimetry,”Advances in Colloid and Interface Science, vol. 76-77, pp. 41–372, 1998.
53. A. G. A. Coombes, S. C. Rizzi, M. Williamson, J. E. Barralet, S. Downes, and W. A. Wallace, “Precipitation casting of polycaprolactone for applications in tissue engineering and drug delivery,” Biomaterials, vol. 25, no. 2, pp. 315–325, 2004.
54. K. Whang, K. E. Healy, D. R. Elenz et al., “Engineering bone regeneration with bioabsorbable scaffolds with novel microarchitecture,” Tissue Engineering, vol. 5, no. 1, pp. 35–51, 1999.
55. J. H. Brauker, V. E. Carr-Brendel, L. A.Martinson, J. Crudele, W. D. Johnston, and R. C. Johnson, “Neovascularization of synthetic membranes directed by membrane micro architecture,”Journal of Biomedical Materials Research, vol. 29, pp.1517–1524, 1995.
56. S. Yang, K. F. Leong, Z. Du, and C. K. Chua, “The design of scaffolds for use in tissue engineering—part I: traditional factors,” Tissue Engineering, vol. 7, no. 6, pp. 679–689, 2001.
57. G. Khang, J. H. Jeon, J.W. Lee, S. C. Cho, and H. B. Lee, “Cell and platelet adhesions on plasma glow discharge-treated poly(lactide-co-glycolide),” Bio-Medical Materials and Engineering, vol. 7, no. 6, pp. 357–368, 1997.
58. K. S. Anseth, C. N. Bowman, and L. Brannon-Peppas, “Mechanical properties of hydrogels and their experimental determination,” Biomaterials, vol. 17, no. 17, pp. 1647–1657, 1996.
59. Einhorn TA: The cell and molecular biology of fracture healing. Clin Orthop Relat Res 1998, 355(Suppl):S7-21.
60. Cho TJ, Gerstenfeld LC, Einhorn TA: Differential temporal expression of members of the transforming growth factor beta superfamily during murine fracture healing. J Bone Miner Res 2002, 17:513-520.
61. Audigé L, Griffin D, Bhandari M, Kellam J, Rüedi TP: Path analysis of factors for delayed healing and nonunion in 416 operatively treated tibial shaft fractures. Clin Orthop Relat Res 2005, 438:221-232.

62. Anto´nio J. Salgado,*1,2 Olga P. Coutinho,1,3 Rui L. Reis1,2., Bone Tissue Engineering: State of the Art and Future Trends
63. H. M. Blau, T. R. Brazelton, J. M. Weimann, Cell 2001,105, 829.
64. Haller AV. Opera Minora. Francisci Grasset1763.
65. Jones A, Harris AL. New developments in angiogenesis: a major mechanism for tumor growth and target for therapy. Cancer J Sci Am 1998 ; 4(4): 209-17.
66. Hobson B, Denekamp J. Endothelial proliferation in tumours and normal tissues: continuous labelling studies. Br J Cancer 1984; 49(4): 405-13.
67. Scherberich A, Galli R, Jaquiery C, Farhadi J, Martin I. Threedimensional perfusion culture of human adipose tissue-derived endothelial and osteoblastic progenitors generates osteogenic constructs with intrinsic vascularization capacity. Stem Cells 2007; 25(7): 1823-9.
68. Ami R.Amini, Cato T.Laurencin, Syam Nukavarapu., Bone Tissue Engineering: Recent Advantages and Challenges.
69. Baroli B. From natural bone grafts to tissue engineering therapeutics: brainstorming on pharmaceutical formulative requirements and challenges.
70. Mirjam Frohlich, Warren L. Grayson, Leo Q. Wan, Darja Marolt, Matej Drobnic, and Gordana Vunjak-Novakovic., Tissue Engineered Bone Grafts: Biological Requirements, Tissue Culture and Clinical Relevance.
71. T. Andric, A.C. Sampson J.W. Freeman,. Fabrication and characterization of electrospun osteon mimicking scaffolds for bone tissue engineering.
72. Wikipedia.
73. Jae-Young Rho, Liisa Kuhn-Spearing, Peter Zioupos,. Mechanical properties and the hierarchial structure of bone.
74. Taylor, B., Dissertation, The development and characterization of an osteoinductive pre-vascularized scaffold for bone tissue regeneration.
75. Z.A.Shazni M.Mariatti A.Nurazreena K.A.Razak., Properties of Calcium Phosphate Scaffolds Produced by Freeze-Casting
76. Ehsan Jabbarzadeh1,2, James Blanchette1, Tarek Shazly3, Ali Khademhosseini4,5,6, Gulden Camci-Unal4,5 and Cato T. Laurencin7,8*., Vascularization of Biomaterials for Bone Tissue Engineering: Current Approaches and Major Challenges.
77. Susmita Bose, Mangal Roy, and Amit Bandyopadhyay., Recent advances in bone tissue engineering scaffolds.
78. Rozalia Dimitriou1,2†, Elena Jones3†, Dennis McGonagle3† and Peter V Giannoudis1,2*†., Bone regeneration: current concepts and future directions.
79. T.Serra[a]J.A.Planell[abc]M.Navarro., High-resolution PLA-based composite scaffolds via 3-D printing technology.